

## Searching for Bumps in the Cosmological Road: Do Type Ia Supernovae with Early Excesses Have Biased Hubble Residuals?

CHRISTINE YE,<sup>1</sup> DAVID O. JONES,<sup>2,3</sup> WILLEM B. HOOGEN DAM,<sup>4,\*</sup> BENJAMIN J. SHAPPEE,<sup>4</sup> SUHAIL DHAWAN,<sup>5</sup> AND SAMMY N. SHARIEF<sup>6</sup>

<sup>1</sup>*Stanford University, 450 Jane Stanford Way, Stanford, CA 94305, USA*

<sup>2</sup>*Gemini Observatory, NSF's NOIRLab, 670 N Aohoku Pl, Hilo, HI, 96720*

<sup>3</sup>*Institute for Astronomy, University of Hawai'i, 640 N. Aohoku Pl., Hilo, HI 96720, USA*

<sup>4</sup>*Institute for Astronomy, University of Hawai'i, 2680 Woodlawn Dr., Honolulu, HI 96822, USA*

<sup>5</sup>*Institute of Astronomy and Kavli Institute for Cosmology, University of Cambridge, Madingley Road, Cambridge CB3 0HA, UK*

<sup>6</sup>*Department of Astronomy, University of Illinois at Urbana Champaign, 1002 W. Green St., IL 61801, USA*

(Dated: February 7, 2024)

### ABSTRACT

Flux excesses in the early time light curves of Type Ia supernovae (SNe Ia) are predicted by multiple theoretical models and have been observed in a number of nearby SNe Ia over the last decade. However, the astrophysical processes that cause these excesses may affect their use as standardizable candles for cosmological parameter measurements. In this paper, we perform a systematic search for early-time excesses in SNe Ia observed by the Zwicky Transient Facility (ZTF) to study whether SNe Ia with these excesses yield systematically different Hubble residuals. We analyze two compilations of ZTF SN Ia light curves from its first year of operations: 127 high-cadence light curves from Yao et al. (2019) and 305 light curves from the ZTF cosmology data release of Dhawan et al. (2022). We detect significant early-time excesses for 17 SNe Ia in these samples and find that the excesses have an average  $g-r$  color of  $0.06 \pm 0.09$  mag; we do not find a clear preference for blue excesses as predicted by several models. Using the SALT3 model, we measure Hubble residuals for these two samples and find that excess-having SNe Ia may have lower Hubble residuals (HR) after correcting for shape, color, and host-galaxy mass, at  $\sim 2-3\sigma$  significance; our baseline result is  $\Delta HR = -0.056 \pm 0.026$  mag ( $2.2\sigma$ ). We compare the host-galaxy masses of excess-having and no-excess SNe Ia and find they are consistent, though at marginal significance excess-having SNe Ia may prefer lower-mass hosts. Additional discoveries of early excess SNe Ia will be a powerful way to understand potential biases in SN Ia cosmology and probe the physics of SN Ia progenitors.

### 1. INTRODUCTION

Type Ia supernovae (SNe Ia), the thermonuclear explosions of white dwarfs (Hoyle & Fowler 1960), are highly standardizable distance indicators, making them powerful tools for precision cosmology (Riess et al. 1998; Perlmutter et al. 1999). However, while it is generally understood that SNe Ia occur from white dwarfs with binary companions, there is still uncertainty around how to explain the diverse range of observable SN Ia properties with different progenitor and explosion models (for reviews, see Maoz et al. 2014; Maeda & Terada 2016; Livio & Mazzali 2018; Jha et al. 2019). Importantly, if observational details (i.e., intrinsic brightness,

color/shape calibration, etc.) vary as a function of galaxy properties or cosmic time, this could introduce systematic changes in their inferred distance measurements that have consequences for the accuracy of SN Ia-based cosmology experiments, especially if the population is changing with redshift (e.g., Childress et al. 2014; Jones et al. 2018; Rose et al. 2019; Rigault et al. 2020; Brout & Scolnic 2021; Nicolas et al. 2021; Kelsey et al. 2022; Thorp & Mandel 2022; Kelsey et al. 2023; Wiseman et al. 2023).

In recent years, measurements of cosmological parameters such as the Hubble Constant ( $H_0$ ) and the dark energy equation of state parameter ( $w$ ) have become increasingly precise (Betoule et al. 2014; Riess et al. 2016; Burns et al. 2018; Scolnic et al. 2018; Freedman et al. 2019; Jones et al. 2019; Brout et al. 2022; Riess et al. 2022; Dhawan et al. 2023; Garnavich et al. 2023; Ru-

\* NSF Graduate Research Fellow

bin et al. 2023; Uddin et al. 2023). As these measurements have improved, indications of a  $>5\sigma$  tension in  $H_0$  between late-universe (Riess et al. 2022) and early-universe (Planck Collaboration et al. 2018) experiments has appeared. This discrepancy potentially implies the existence of new physics (see Di Valentino et al. 2021 for a review) and motivates the need for even more robust measurements in the coming years. For example, systematic uncertainties in SN Ia distances — though they are highly unlikely to be of a size that resolves the  $H_0$  tension (Dhawan et al. 2020) — could stem from coincidental or systematic mismatches between SN Ia properties in different rungs of the  $H_0$  distance ladder. Similarly, changes in SN Ia properties across cosmic time have the potential to affect  $w$  (e.g., Pan et al. 2022).

As an example of such a systematic on  $w$ , an overluminous subpopulation of SNe Ia would produce relative underestimates of distances. While such SNe Ia may be rare in the local universe (Desai et al. 2023), they may be more common at higher redshifts as cosmic metallicity decreases (e.g., Domínguez et al. 2001), thereby affecting measurements of  $w$ . The discovery of the (still poorly understood) dependence of SN Ia distance measurements on the masses of their host galaxies (Kelly et al. 2010; Lampeitl et al. 2010; Sullivan et al. 2010) is one previous systematic error in SN Ia distances that affected both  $w$  and  $H_0$  measurements (Sullivan et al. 2011; Riess et al. 2016).

Such systematics are not well constrained from a theoretical perspective; models for SNe Ia vary in the progenitor system (e.g., whether the companion is a white dwarf or a nondegenerate star; Whelan & Iben 1973; Iben & Tutukov 1984; Webbink 1984; Livne 1990; Nomoto et al. 1997), and/or the explosion mechanism (e.g., Whelan & Iben 1973; Nomoto 1980; Iben & Tutukov 1984; Woosley & Weaver 1994; Hoefflich & Khokhlov 1996; Piersanti et al. 2003; van Kerkwijk et al. 2010; Diamond et al. 2018). But while most physical models of SNe Ia generate indistinguishable predictions near maximum light, some disagree in their predictions for very early times post explosion (the first hours to days) and the very late time evolution (e.g., Ashall et al. 2019; Kumar et al. 2023).

For example, in the single-degenerate case, the SN Ia ejecta may collide with the companion star, which becomes shock-heated and results in a blue/UV excess in the first 5 days after explosion that is observable in  $\sim 10 - 20\%$  of events (Marietta et al. 2000; Kasen 2010; Burke et al. 2022b,a; Deckers et al. 2022). However, Hoogendam et al. (2023) find that companion interaction is unlikely to explain the diversity of observed excesses; alternatively, models with circumstellar material,

double-detonation mechanisms (an outer shell detonation that triggers a detonation in the core; Fink et al. 2007), or radioactive matter in the outer ejecta (e.g., Jiang et al. 2018) also predict early excesses, although often with distinct color/spectral evolution (Piro 2012; Piro & Morozova 2016; Contreras et al. 2018; Maeda et al. 2018; Polin et al. 2019; Magee et al. 2020; Magee & Maguire 2020).

Prior to  $\sim 2010$ , few SNe Ia could be observed with sufficient cadence or depth at early times to observe such signatures. However, over the last decade, there have been numerous reports of SNe Ia with early-time behavior that is inconsistent with a simple power-law rise. Some notable examples from the literature are SN 2012cg (Marion et al. 2016, but also see Shappee et al. 2018), SN 2012fr (Contreras et al. 2018), SN 2014J (Goobar et al. 2015; Siverd et al. 2015), SN 2016jhr (Jiang et al. 2017), SN 2017cbv (Hosseinzadeh et al. 2017), SN 2018oh (Dimitriadis et al. 2019; Li et al. 2019; Shappee et al. 2019), SN 2021aefx (Ashall et al. 2022; Hosseinzadeh et al. 2022) and, most recently, SN 2023bee (Hosseinzadeh et al. 2023; Wang et al. 2023), all of which exhibit a monotonic “excess” above the power-law expectation, before a steeper power-law rise in luminosity. Reported excesses occur in normal, overluminous, and underluminous SNe, at UV, blue, and/or red wavelengths (Stritzinger et al. 2018, e.g.), and with varied shapes (e.g., Fausnaugh et al. 2023).

Other early-excess SNe Ia exhibit non-monotonic “bumps,” declining slightly before the power-law rise, such as SN iPTF14atg (Kromer et al. 2016), SN 2019yvq (Miller et al. 2020), SN 2020hvf (Jiang et al. 2021), SN 2021zny (Dimitriadis et al. 2023), and SN 2022ilv (Srivastav et al. 2023). Presently, only 2002es-like and 2003fg-like SNe Ia have observed bumps, and while the ultraviolet colors show significant differences between bump and other SNe Ia, the optical colors are indistinguishable between the two categories, suggesting that differing mechanisms produce “excess” and “bump” SNe Ia (Hoogendam et al. 2023).

Given the potential for different physics in these early-excess explosions, possibly leading to systematic biases, it is important to check whether their distance measurements can reliably be used for cosmology. In this paper, we examine whether SNe Ia with early excesses have systematic offsets in their distance measurements compared to non-excess SNe Ia, by systematically identifying SNe Ia with early excesses in Zwicky Transient Facility light curves (ZTF; Bellm et al. 2019). We also search for population differences between SNe Ia with and without early excesses.

The text is organized as follows: in Section 2 we describe the light-curve fitting and sample selection procedures; in Section 3 we detail criteria for excess and no-excess SNe Ia; and in Section 4 we discuss and compare our results. In Section 5 we discuss caveats and implications of our results. Section 6 summarizes the results of the work and provides concluding remarks.

## 2. SAMPLE SELECTION

### 2.1. ZTF Data

The dataset used in this paper is taken from observations by the Zwicky Transient Facility (ZTF) in 2018 (Bellm et al. 2019; Masci et al. 2019). We also investigate the  $z < 0.05$  ZTF SNe Ia sample from 2019–2022, but exclude it from our analysis due to higher scatter in the Hubble residuals (future data releases will likely improve the fidelity of the light-curves for cosmological measurements) and a lack of early excess detections.

ZTF detects astronomical transients in an untargeted, high-cadence survey covering the  $g, r,$  and  $i$  bands. At the time of the 2018 observations, ZTF’s Mid-Scale Innovations Program (MSIP) survey was covering approximately  $13,000 \text{ deg}^2$  per night in the  $gr$  bands at a cadence of three days (the ZTF phase II survey, which commenced in late 2020, has a two-day cadence). Additionally, ZTF conducted an  $i$ -band survey across  $\sim 8000 \text{ deg}^2$  with a four-day cadence and a one-day cadence survey in  $gr$  across  $\sim 1700 \text{ deg}^2$ . Additional information about the ZTF surveys is given by Bellm et al. (2019).

We use data published by Yao et al. (2019) and Dhawan et al. (2022), which is from a combination of the ZTF surveys described above. The Yao et al. (2019) sample specifically selects SNe Ia with high-S/N, high-cadence early time light curves. They use point spread function (PSF) fitting (Masci et al. 2019), with the centroid fixed at the average SN Ia location, to produce light curves for 127 SNe Ia with detections earlier than 10 rest-frame days before maximum light, including 50 objects with detections earlier than 14 rest-frame days before maximum light. In addition to the Yao et al. (2019) analysis, the early time behavior of SNe Ia in this sample has also been investigated by Burke et al. (2022b) and Deckers et al. (2022). This sample has a median redshift of  $z = 0.074$ .

The Dhawan et al. (2022) analysis, from a total of 761 spectroscopically classified SNe Ia that were observed in 2018, re-reduces 305 SNe Ia with host-galaxy redshifts using a new photometric pipeline intended for cosmological analyses. The median redshift is  $z = 0.057$ .

Due to the poor sampling and reduced depth of  $i$  band data, we consider only  $g$  and  $r$  light curves for identifying early excesses.

### 2.2. Light-curve Fitting for Cosmology

We use the Python package SNeCosmo to perform light-curve fitting with the SALT3 spectral energy distribution model (Kenworthy et al. 2021; Taylor et al. 2023). SALT3 improves upon previous generations of SALT (Spectral Adaptive Light-curve Template; Guy et al. 2005, 2007) models with an expanded training sample and better handling of uncertainties. We correct for Milky Way dust extinction using the Schlafly & Finkbeiner (2011) reddening maps. With redshifts from host galaxies (where available) or SN Ia spectra, SALT3 fitting produces estimates for  $x_0$ , an overall amplitude parameter;  $x_1$ , the first principal component of variation, which correlates with shape;  $c$ , a color parameter; and  $t_0$ , the time of light-curve peak.  $m_B$ , the apparent  $B$ -band magnitude at peak, is directly estimated from SALT3  $x_0$ :  $m_B = -2.5 \log_{10} x_0 + 10.635 \text{ mag}$ .

### 2.3. Host-galaxy Mass Determination

Due to the observed dependence of SN Ia standardized magnitudes on the host-galaxy stellar mass of a SN Ia (Kelly et al. 2010; Lampeitl et al. 2010; Sullivan et al. 2010), SN Ia distance determinations must include host galaxy identifications and mass estimates. Here, we match each SN Ia to its most likely host galaxy using the Galaxies HOsting Supernovae and other Transients (GHOST; Gagliano et al. 2021) software. GHOST applies a gradient ascent method to postage-stamp images of each SN Ia location to find the most likely host galaxy for the SN.

GHOST also provides Pan-STARRS catalog photometry (Flewelling et al. 2020) for these hosts, which we supplement with Sloan Digital Sky Survey (SDSS; York et al. 2000) photometry when Pan-STARRS magnitudes are not available (Pan-STARRS images exist at every location with SDSS imaging, but we found that catalog photometry for a give source is sometimes unavailable). In the rare cases when Pan-STARRS images exist, but Pan-STARRS and SDSS catalog magnitudes do not, we use elliptical aperture photometry within the isophotal radius to measure the galaxy’s magnitudes from the Pan-STARRS images directly.

Galaxy masses were estimated using  $g$  and  $i$  band Kron magnitudes from the relation given by Taylor et al. (2011):

$$\log M_*/[M_\odot] = 1.15 + 0.7(g - i) - 0.4(i - \mu(z)) \quad (1)$$

with  $\mu(z)$  from Planck Collaboration et al. (2018) cosmology. SNe Ia for which a host galaxy cannot be identified visually or with GHOST are assigned a host-galaxy mass  $< 10 \text{ dex}$ .

#### 2.4. Distances and Cosmological Sample Selection

For each SN, we estimate the distance modulus,  $\mu$ , from SALT3 parameters using the Tripp equation (Tripp 1998):

$$\mu = m_B + \alpha x_1 - \beta c - \mathcal{M}(z) + \gamma \mathcal{H}(M_\odot - 10), \quad (2)$$

where  $\alpha$  and  $\beta$  are nuisance parameters that relate the  $x_1$  and  $c$  parameters to  $\mu$ ,  $\gamma$  is the size of the host-galaxy mass step, and  $\mathcal{H}$  is the Heaviside step function.  $\mathcal{M}$  is the SNIa absolute magnitude (degenerate with  $H_0$ ).

To remove any dependence of the Hubble residuals on redshift, including dependence on the cosmological model and distance-dependent selection effects (e.g., Kessler & Scolnic 2017), we fit  $\mathcal{M}(z)$  as a piecewise function with independent values for  $\mathcal{M}(0 < z \leq 0.033)$ ,  $\mathcal{M}(0.033 < z \leq 0.067)$ , and  $\mathcal{M}(0.067 < z \leq 0.1)$ .

The uncertainty on  $\mu$ ,  $\sigma_\mu$ , is:

$$\begin{aligned} \sigma_\mu^2 = & \sigma_{int}^2 + \sigma_{\mu,z}^2 + \sigma_{m_B}^2 + (\alpha\sigma_{x_1})^2 + (\beta\sigma_c)^2 \\ & + 2\alpha\beta\sigma_{c,x_1} + 2\alpha\sigma_{m_B,x_1} + 2\beta\sigma_{m_B,c}. \end{aligned} \quad (3)$$

We adopt  $\sigma_{lens} = 0.055z$  following Jönsson et al. (2010) and the covariances/errors  $\sigma_{c,x_1}$ ,  $\sigma_{m_B,x_1}$ ,  $\sigma_{m_B,c}$ ,  $\sigma_{x_1}$ ,  $\sigma_c$  from the SALT3 fits. The intrinsic dispersion,  $\sigma_{int}$ , is the remaining scatter of SNIa Hubble residuals after photometric and model uncertainties have been taken into account. Corrections for the effect of local overdensities (peculiar velocities) are estimated from 2M++ (Carrick et al. 2015), with uncertainties on the corrections of  $250 \text{ km s}^{-1}$  (Scolnic et al. 2018).

To standardize our sample, we impose the following selection requirements following previous SNe Ia cosmology analyses (e.g., Brout et al. 2022). To be included, SNe Ia must have:

1. Normal or 1991T-like spectroscopic classifications.
2. At least 3 data points between  $-10$  and  $10$  days.
3. Well-constrained shape:  $\sigma_{x_1} < 1$ .
4. Multiple filters (both  $g$  and  $r$ ) to constrain the color parameter and  $\sigma_c < 0.3$ .
5. Well-constrained peak epoch:  $\sigma_{t_0} < 1$ .
6. The  $x_1$  parameter is consistent with a normal SNIa:  $-3 < x_1 < 3$ .
7. Color parameter consistent with a normal SNIa that is not highly reddened:  $-0.3 < c < 0.3$ .

8. Chauvenet’s criterion: SNe Ia with less than a 50% chance of belonging to the observed, normally-distributed SNIa population. This selection criterion is computed from the sample size and Hubble residual dispersion of our data and removes one SNIa from each of the Yao et al. (2019) and Dhawan et al. (2022) samples.

We also include a redshift cut of  $0.01 < z < 0.1$ , to ensure that peculiar velocities don’t dominate the Hubble residual uncertainty at the low-redshift end, and to limit cosmological model sensitivity and distance biases at the high-redshift end.

After these cuts, we are left with 194/305 SNe Ia from the Dhawan et al. (2022) sample and 88/127 SNe Ia from the Yao et al. (2019) sample. We simultaneously fit estimates of  $\alpha$ ,  $\beta$ ,  $\gamma$ ,  $\mathcal{M}(z)$ , and  $\sigma_{int}$  to both samples. The results are presented in Table 1. Although the intrinsic dispersion is higher than usual for a SNIa sample (typically  $\sim 0.1$ - $0.12$  mag), the total r.m.s. of the Hubble residuals is not; this is most likely an indication of under-estimated photometric errors. We note that the Yao et al. (2019) and Dhawan et al. (2022)  $\beta$  parameters are slightly inconsistent with each other, with the Yao et al. (2019) value slightly closer to a typical SALT3 value (Kenworthy et al. 2021). This may be due to a color-dependent calibration error or selection effects, which differ substantially between the two samples and result in significantly different values for  $\mathcal{M}(z)$ ; we discuss potential inconsistencies between the samples and possible implications of miscalibration on our results in Section 5.

### 3. EARLY EXCESS FITTING

#### 3.1. Models

In the first few days after explosion, we would expect the flux of SNe Ia to follow a power-law rise of roughly  $f \propto t^2$  under the assumption of a constant-temperature photosphere expanding at a constant rate (the so-called expanding fireball model; Riess et al. 1999). Indeed, studies have shown that this holds approximately true at least 10-15 days before maximum light (Miller et al. 2020), although there are some notable exceptions (e.g., Shappee et al. 2016; Fausnaugh et al. 2023; Hoogendam et al. 2023). At later times, closer to maximum light, the slope decreases. For SNe Ia with detected early excesses, multiple functional forms for light-curve fits have been recorded in the literature, including double power laws (e.g., Shappee et al. 2019), single power laws with a Gaussian component (e.g., Dimitriadis et al. 2019), and physically motivated models; for example, Hosseinzadeh et al. (2023) fits light curves with a single-degenerate



Data	$\alpha$	$\beta$	$\mathcal{M}$ (mag)	$\gamma$ (mag)	$\sigma_{int}$ (mag)	rms (mag)
Dhawan et al. (2022)	$0.118 \pm 0.009$	$2.54 \pm 0.08$	$-19.07 \pm 0.02, -19.16 \pm 0.02, -19.21 \pm 0.02$	$0.05 \pm 0.02$	0.144	0.152
Yao et al. (2019)	$0.109 \pm 0.004$	$2.773 \pm 0.004$	$-19.25 \pm 0.05, -19.16 \pm 0.03, -19.18 \pm 0.02$	$0.04 \pm 0.05$	0.149	0.153

**Table 1.** Nuisance parameters for SNe Ia in the two public samples analyzed in this work.  $\mathcal{M}$  is listed in order of increasing redshift range:  $[0 < z \leq 0.033, 0.033 < z \leq 0.067, 0.067 < z \leq 0.1]$ .

model that depends on parameters such as progenitor radius and shock velocity.

After testing multiple fitting procedures on SNe Ia with known excesses, we find that a two-component (Gaussian and Power Law, hereafter the Gaussian+PL model) model offers sufficient flexibility in fitting all observed excesses, while also allowing for quantitative measures of the significance of the excess. This formulation also more directly corresponds to physical parameters in the system, such as the total amount of energy in the early excess, as compared to other analytic models. We characterize early light curves for a given band  $b$  as follows:

$$f_b(t) = B_b + \mathcal{H}(t_{exp})A_b(t - t_{exp})^{\alpha_b} + C_b\mathcal{N}(\mu, \sigma) \quad (4)$$

where  $B_b$  is a constant offset,  $t_{exp}$  refers to the time of first light from the explosion,  $\mu$  and  $\sigma$  are the location and standard deviation of the Gaussian component,  $A_b$  is the power-law scale factor in a given band,  $\alpha_b$  is a band-dependent power-law exponent, and  $C_b$  is the Gaussian scale factor in a given band.  $\mathcal{H}$  is the Heaviside step function, equal to zero before  $t_{exp}$  and a constant afterwards. In total, we have 9 parameters, which we fit for using least-squares minimization with constraints set in Table 2.

**Table 2.** Constraints on Early Excess Fitting Parameters

$B_r$	[-100.0, 100.0]
$B_g$	[-100.0, 100.0]
$A_r$	[0.0, 500.0]
$A_g$	[0.0, 500.0]
$t_{exp}$	$[t_0 - 40, t_0 - 10]$
$\alpha_r$	[1.0, 3.0]
$\alpha_g$	[1.0, 3.0]
$\mu$	$[t_{exp}, t_{exp} + 5]$
$\sigma$	[0.5, 4.0]
$C_r$	[0.0, 500.0]
$C_g$	[0.0, 500.0]

The parameter  $t_0$  is the time of maximum light in the  $B$  band, which we estimate using SALT3. We constrain  $\mu$  to  $[t_{exp}, t_{exp} + 5]$  because we are only searching for

early excesses, and  $\alpha$  to [1.0, 3.0] based on predicted and observed power-law light curve rises.

We also fit power-law-only (hereafter PL-only) models to the data to test whether a Gaussian component is truly necessary. These models have seven parameters ( $A_r, A_g, B_r, B_g, \alpha_r, \alpha_g, t_{exp}$ ).

For each SNe Ia, we fit using the light-curve data between  $t_0 - 40$  and  $t_0 - N$ , where  $N$  ranges between 7 to 14 days. Allowing variation in  $N$  between individual SNe Ia allows us to maximize the number of included data points while avoiding later epochs when the power-law flux model is no longer a valid approximation. The ideal value of  $N$  is usually around  $\sim 9 - 10$  days. We visually inspect each identified early excess to ensure that the latest fitted epochs remain consistent with the best-fit power law.

### 3.2. Criteria for Detecting an Early Excess

To systematically search for early-time excesses in SNe Ia, we require SNe Ia with potential early excesses to pass a number of statistical tests confirming their credibility. These specific criteria are given in the Appendix (A) and summarized below. First, we check the quality and sampling of the light curve data, requiring that a substantial number of data points exist immediately pre- and post-explosion. In case excesses that appear statistically significant are due to poor light curve fits or underestimated flux errors, we also remove SNe Ia having fits with high reduced  $\chi^2$  and/or individual extreme outliers. We measure the statistical significance of the early excess from the significance of the model fit's Gaussian component, and we visually inspect each light curve with a statistically significant excess as a final check on the quality of the data and the fit.

Moreover, models with more parameters will tend to fit any light curve better than models with fewer parameters, whether or not the additional parameters are actually necessary. Thus in order to calculate whether the Gaussian+PL model is truly favored over the PL-only model, we use the Bayesian Information Criterion (BIC), which penalizes models with more parameters:

$$\text{BIC} = k \ln(n) - 2 \ln(\hat{L}), \quad (5)$$

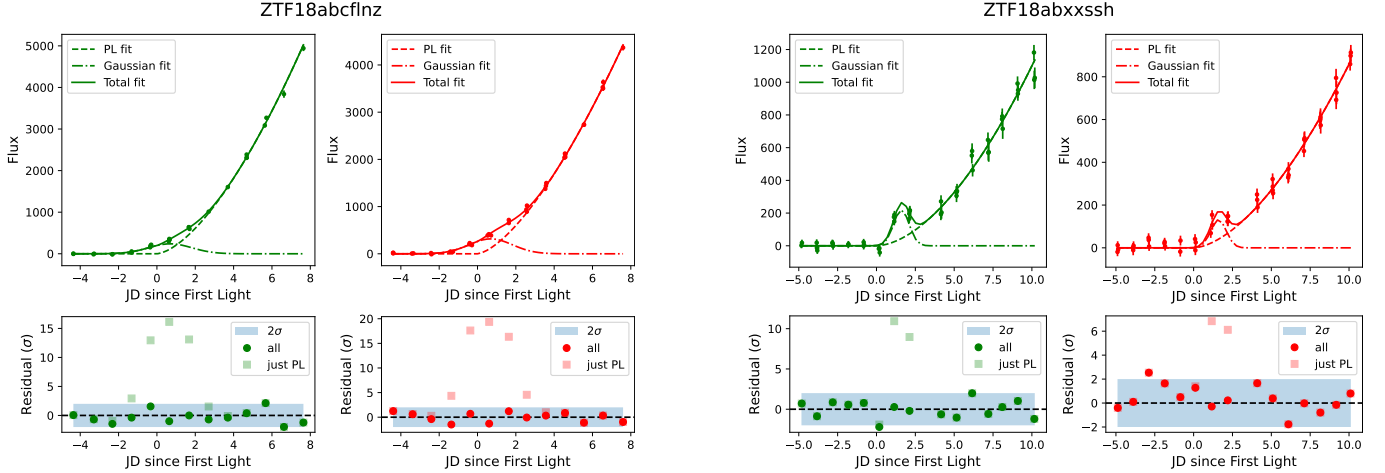


**Figure 1.** Example gold-tier detections of bump early excesses. Panels display light curves in ZTF  $g$  (green; left) and  $r$  (red; right) bands, respectively. Points represent actual observations, while the lines represent fitted models: the power-law component (dashed), the Gaussian component (dash-dotted), and the total fit (solid). On epochs with multiple observations, the plotted residuals (bottom) are weighted averages. Fluxes are calculated with zero point set at 25.0 mag.

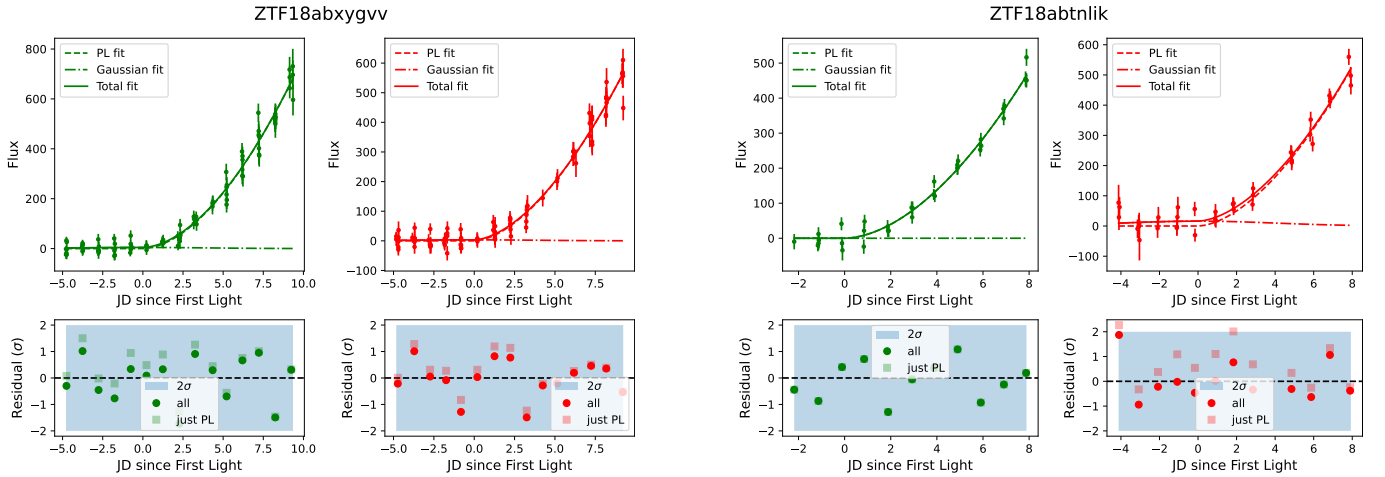


**Figure 2.** Example gold-tier (left panel) and bronze-tier (right panel) non-detections of bump early excesses. Panels display light curves in ZTF  $g$  (green; left) and  $r$  (red; right) bands, respectively. See the Figure 1 caption for additional details.

where  $k$  is the number of parameters,  $n$  is the number of data points, and  $\hat{L}$  is the likelihood. The likelihood, which is assumed to be Gaussian, is given by:

$$\ln \hat{L} = \sum_i^n -\frac{(x_i - f_i(t))^2}{\sigma_{x,i}^2/2} + \ln\left(\frac{1}{\sqrt{2\pi}\sigma_{x,i}^2}\right). \quad (6)$$

Here,  $x_i$  is the  $i$ th flux measurement,  $f_i(t)$  is the model at the time of the  $i$ th flux, and  $\sigma_{x,i}$  is the flux uncertainty.

We also find that there is often a degeneracy between the power-law slope,  $\alpha$ , and the existence of an early excess. An example of these degeneracies for one of our “gold” SNe Ia, ZTF18abxxssh, is shown in Figure 3. Especially if the cadence is sparse, a lower value of  $\alpha$  with

a later explosion date and a non-zero excess component can often fit the data as well as a steeper power law, an earlier explosion date, and no excess component. This is particularly likely if  $N$  is smaller, such that data closer to maximum light are being fit, increasing the chances that the light curve slope is no longer  $\sim t^2$  at the later epochs<sup>1</sup>. In these situations, we use the BIC to judge whether or not the additional “bump” component is pre-

<sup>1</sup> Olling et al. (2015) find that a single power-law fit is a good approximation when the SN Ia flux is less than 40% of its eventual maximum. Our chosen values of  $N$  are approximately in agreement with this cutoff but sometimes limited by data availability in days 0-5, as 40% often corresponds to 5-6 days or earlier post-explosion.

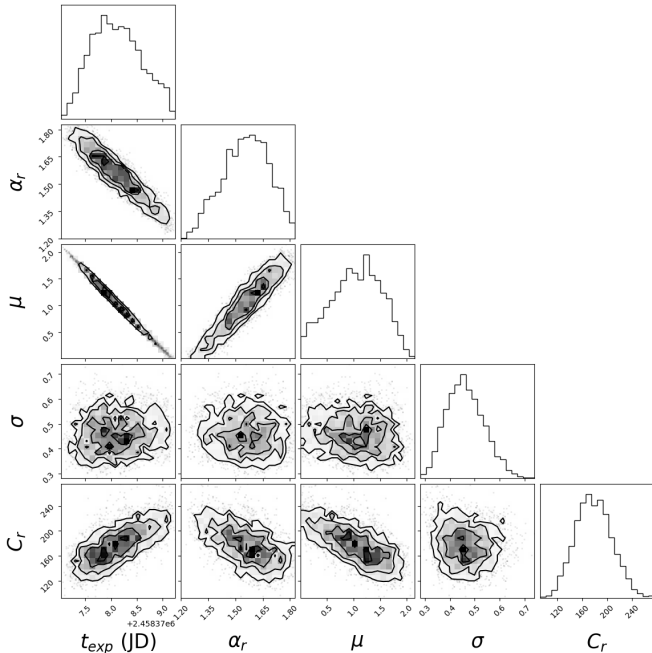


**Figure 3.** Corner plot showing a subset of parameters for ZTF18zzssh using PyMultiNest and `corner` (Buchner et al. 2014; Foreman-Mackey 2016). From left to right: time of explosion ( $t_{exp}$ ),  $r$ -band power-law slope ( $\alpha_r$ ), Gaussian mean ( $\mu$ ), Gaussian width ( $\sigma$ ), and  $r$ -band Gaussian amplitude  $C_r$ . Although the bump is detected with high significance, several correlations between these parameters are evident.

ferred. We also examine whether a potential early excess disappears when stricter bounds on  $\alpha$  are placed, or some of the data nearer to maximum light is excluded (by increasing  $N$ ).

Based on these considerations, we create two sets of criteria — “gold” and “bronze” — for defining different samples of SNe Ia with early excesses. All identified gold and bronze tier SNe Ia from the Yao et al. (2019) and Dhawan et al. (2022) samples are given in Tables 3 and 4. The exact criteria for inclusion in each of these samples is given in the Appendix (A).

The gold tier for non-detections is defined as SNe Ia for which we are confident that no excess exists at the flux limit required for inclusion in the gold sample. However, in much of this analysis we also compare the “gold” or “bronze” excess-having sample to *all* SNe Ia for which an excess has not been detected (either due to the data’s lack of sensitivity or an actual, significant non-detection of a “bump”). For this second sample, we note that if there is a Hubble residual difference between SNe Ia with excesses and those without (Section 4.2), comparing to all SNe Ia without excess detections means that it would appear slightly smaller in this study than it would if we could identify 100% of SNe Ia without early excesses.

However, because literature studies have estimated that just 10-20% of SNe Ia have early excesses (e.g., Burke et al. 2022a), the “no excess” sample should not have a large contaminating fraction of excess-having SNe.

We also considered the possibility that flux errors from forced photometry are underestimated, potentially resulting in the detection of “significant” excesses that are not actually real. To account for this, we test the effect of multiplying the flux uncertainties by an amount such that the reduced  $\chi^2$  of pre-explosion data, compared to the zero-flux expectation, is  $\sim 1$ . We find that this does not impact any claimed excesses from our sample.

Two high-cadence, low-scatter light curves with significant detections of early excesses are shown in Figure 1 and are representative of our gold tier “excess” sample. The remaining gold and bronze light curves are shown in the appendix. Two example light curves with similar cadence and error bars but no “bump” detection are shown in Figure 2 and are representative of our gold tier “no excess” sample. Due to the ZTF cadence, there are often multiple light-curve data points per night; assuming that the SNe Ia flux does not vary drastically within a night, for plotting purposes we bin the residuals by epoch and take their weighted average. Moreover, for clarity, we only plot data points between  $t_{exp} - 5$  and  $t_0 - N$ , but many light curves have long pre-explosion baselines that tightly constrain the epoch of explosion.

## 4. RESULTS

### 4.1. SNe Ia with Excesses

Unsurprisingly, due to the high cadence and exceptional pre-peak coverage, we find that most SNe Ia with significant, detectable early excesses come from the Yao et al. (2019) sample. In total, from the Yao et al. (2019) sample, Burke et al. (2022b) report 11 SNe Ia with early excesses: 2 gold, 4 silver, and 5 bronze. Our models (Section 3) find 14 SNe Ia (4 gold, 10 bronze<sup>2</sup>) with excesses in the same sample, 7 of which overlap with the Burke et al. (2022b) findings. One SNe Ia (ZTF18aayjvve) is previously reported in Deckers et al. (2022); the other 6 SNe Ia (ZTF18abucvbf, ZTF18aasdted, ZTF18abaxlpi, ZTF18abfgygp, ZTF18aaslhxt, ZTF18abauprj), one of which we identify as a gold-tier excess, have not previously been reported. We find just 4 objects that can be classified as gold-tier no-excess SNe Ia due to the difficulty of ruling out bumps smaller than our smallest clear detection in the three-day cadence ZTF data.

<sup>2</sup> We note that these tiers are loosely modeled after Burke et al. (2022b), but use the criteria discussed in Section 3.2 and the Appendix.

ZTF ID	$z$	$t_0$	$m_B$ (mag)	$x_1$	$c$	$\Delta$ BIC	$f_{b,r}/f_{10,r}$	$f_{b,g}/f_{10,g}$	$N$
Gold Tier									
aayjvve	0.047	58292.3	$17.655 \pm 0.005$	$-0.18 \pm 0.03$	$0.052 \pm 0.004$	27	$0.07 \pm 0.02$	$0.05 \pm 0.01$	8
abcflnz	0.027	58306.2	$16.110 \pm 0.003$	$-0.04 \pm 0.01$	$-0.024 \pm 0.002$	31	$0.03 \pm 0.01$	$0.02 \pm 0.01$	9
abucvbf	0.055	58385.0	$17.524 \pm 0.003$	$-0.37 \pm 0.04$	$-0.091 \pm 0.003$	36	$0.05 \pm 0.01$	$0.04 \pm 0.01$	8
abxxssh	0.078	58397.4	$18.221 \pm 0.01$	$1.51 \pm 0.10$	$-0.035 \pm 0.007$	91	$0.14 \pm 0.10$	$0.20 \pm 0.10$	10
Bronze Tier									
aasdted	0.018	58265.5	$15.838 \pm 0.002$	$0.83 \pm 0.01$	$0.166 \pm 0.002$	120	$0.03 \pm 0.03$	$0.02 \pm 0.03$	8
aaslhxt	0.055	58263.7	$17.625 \pm 0.003$	$0.36 \pm 0.02$	$-0.116 \pm 0.002$	12	$0.05 \pm 0.03$	$0.05 \pm 0.03$	8
aaxsioa	0.032	58286.2	$16.884 \pm 0.002$	$-1.61 \pm 0.01$	$0.063 \pm 0.002$	-5	$0.03 \pm 0.08$	$0.00 \pm 0.01$	7
aazsabq	0.060	58294.0	$18.233 \pm 0.004$	$-1.46 \pm 0.03$	$0.033 \pm 0.004$	-10	$0.04 \pm 0.03$	$0.01 \pm 0.01$	8
abauprj	0.024	58302.6	$15.526 \pm 0.002$	$1.37 \pm 0.02$	$-0.012 \pm 0.002$	299	$0.03 \pm 0.00$	$0.02 \pm 0.00$	9
abaxlpi	0.064	58298.5	$18.394 \pm 0.005$	$0.12 \pm 0.05$	$0.047 \pm 0.004$	24	$0.06 \pm 0.07$	$0.05 \pm 0.06$	9
abfgygp	0.064	58322.0	$18.032 \pm 0.003$	$-0.01 \pm 0.02$	$-0.076 \pm 0.003$	2	$0.09 \pm 0.02$	$0.07 \pm 0.01$	9
abfhryc	0.032	58323.9	$16.468 \pm 0.003$	$0.50 \pm 0.02$	$-0.014 \pm 0.002$	99	$0.06 \pm 0.05$	$0.05 \pm 0.04$	11
abimsyv	0.088	58334.5	$18.540 \pm 0.006$	$1.04 \pm 0.04$	$-0.046 \pm 0.004$	-5	$0.04 \pm 0.03$	$0.06 \pm 0.03$	9
abssuxz	0.065	58377.0	$18.155 \pm 0.008$	$-2.10 \pm 0.10$	$0.027 \pm 0.007$	-11	$0.05 \pm 0.07$	$0.07 \pm 0.05$	4

**Table 3.** SNeIa with early excesses and their SALT3 properties from the Yao et al. (2019) sample. Bump properties are quoted at a reasonable, BIC-maximizing  $N$ .  $f_b$  refers to the maximum excess bump flux, whereas  $f_{10}$  refers to the flux at 10 days post-explosion, in each band. Typical errors on  $z$  and  $t_0$  are less than  $10^{-3}$  and  $10^{-1}$ , respectively.

ZTF ID	$z$	$t_{exp}$	$m_B$ (mag)	$x_1$	$c$	$\Delta$ BIC	$f_{b,r}/f_{10,r}$	$f_{b,g}/f_{10,g}$	$N$
Gold Tier									
aayjvve	0.047	58292.2	$17.704 \pm 0.005$	$-0.08 \pm 0.04$	$0.065 \pm 0.004$	16	$0.08 \pm 0.03$	$0.06 \pm 0.02$	7
abauprj	0.024	58302.2	$15.556 \pm 0.001$	$1.34 \pm 0.01$	$-0.033 \pm 0.001$	93	$0.02 \pm 0.01$	$0.02 \pm 0.01$	12
Bronze Tier									
abkhwcl	0.032	58344.3	$16.426 \pm 0.003$	$0.01 \pm 0.02$	$-0.092 \pm 0.002$	8	$0.00 \pm 0.10$	$0.10 \pm 0.10$	8
abuhzfc	0.037	58383.0	$17.239 \pm 0.004$	$-0.78 \pm 0.06$	$0.139 \pm 0.004$	2	$0.02 \pm 0.02$	$0.20 \pm 0.20$	8
abvejbm	0.044	58385.8	$17.250 \pm 0.010$	$-2.14 \pm 0.05$	$-0.010 \pm 0.009$	3	$0.05 \pm 0.04$	$0.04 \pm 0.04$	8

**Table 4.** SNeIa with early excesses and their SALT3 properties from the ZTF 2018 cosmology sample. Bump properties are quoted at reasonable, BIC-maximizing  $N$ .  $f_b$  refers to the maximum excess bump flux, whereas  $f_{10}$  refers to the flux at 10 days post-explosion, in each band. SNeIa ZTF18aayjvve and ZTF18abauprj are also found in the Yao et al. (2019) sample.

With the same systematic criteria, we search for early excesses in the SNeIa light curves from the ZTF 2018 cosmology data release. From the Dhawan et al. (2022) sample, we identify 2 gold-tier and 3 bronze-tier excesses, 2 of which overlap with the excesses found in the previously discussed sample; ZTF18abvejbm and ZTF18abuhzfc are unique to the Dhawan et al. (2022) sample. We find only two objects that can be classified as gold-tier no-excess SNeIa.

For the other early-excess SNeIa found in Burke et al. (2022a) or Yao et al. (2019) with light curves also available in the Dhawan et al. (2022) dataset, we find that the Dhawan et al. (2022) data allowed detection of early excesses in cases where the original ZTF forced photometry light curves were often too poorly sampled to detect them. For SNe that we do not detect excesses in, but have been reported as having early excesses in

other analyses, we remove them our list of gold-tier non-detections. We find  $\sim 1$  gold-tier early excess and  $\sim 5 - 10$  bronze-tier early excesses in the ZTF 2019-2022 sample, but ultimately do not include these SNeIa due to the small number of excess detections and some data quality issues that affected how confident we could be in those detections, including lack of pre-explosion data, template over-subtraction, significant light-curve outliers, and under-estimated uncertainties (it is likely that these light curves will be improved in future data releases).

Overall, SNeIa with early excesses have relatively similar lightcurve shapes  $x_1$  and colors  $c$  compared to SNeIa without them. From the Yao et al. (2019) sample, early-excess SN Ia have  $\bar{x}_1 = -0.100 \pm 0.005$  and  $\bar{c} = 0.0180 \pm 0.0007$ , compared to excess-free SN,  $\bar{x}_1 = -0.798 \pm 0.04$  and  $\bar{c} = 0.0308 \pm 0.0005$ .



#### 4.2. Hubble Residuals

Flux excesses may originate from different SNIa progenitor systems and/or explosion mechanisms such that the cosmological standardization of the SNIa with excesses may be adversely affected. Therefore, it is reasonable to expect that there may be a resulting difference in the measured distance moduli,  $\mu$ , between the excess-having and no-excess SNIa populations. After fitting for Tripp equation nuisance parameters (Section 2.4), including corrections for light-curve shape, color and host-galaxy mass, and marginalizing over redshift-dependent trends in a manner similar to Marriner et al. (2011), we compare Hubble residuals ( $\mu_{SALT3} - \mu_{\Lambda_{CDM}}$ ) for each sample; results are shown in Figure 4.

We begin with the literature sample of SNIa with early excesses identified in Burke et al. (2022a). We combine the Burke et al. (2022a) “gold” and “silver” classifications into a single “gold” tier, and add in the Burke et al. (2022a) “bronze” class for the full population of excess-having SN. The gold-tier no-excess SNIa are taken from our analysis of Yao et al. (2019) light curves, as discussed in Section 3.2. The combined gold-tier and bronze-tier samples, representing all excess-having SNe, when compared to all other SNe, have  $\Delta HR = -0.055 \pm 0.033$  mag, or about  $1.7\sigma$ . Within the gold tier, excess-having SNIa and the gold-tier no-excess sample have comparable Hubble residuals  $\Delta HR = -0.120 \pm 0.066$  mag, although we caution that comparisons within the gold tier are difficult due to low statistics (4 excess and 4 no-excess SNe).

Next, using the same data source as Burke et al. (2022b), detailed in Yao et al. (2019), we use the results of our systematic search for early excesses as described in 3.2. We define new gold and bronze tiers, and find that our identification of SNIa with early excesses is somewhat more conservative than Burke et al. (2022b) (see Section 5 for a discussion of the different samples in this work). We again find that, on a population level, excess-having SNIa have lower Hubble residuals (and are thus brighter); we measure  $\Delta HR = -0.038 \pm 0.030$  mag. This sample shares the same gold-tier non-detection sample (4 SNe) as the Burke et al. (2022b) paper; within this more limited sample, we measure  $\Delta HR = -0.105 \pm 0.072$ .

Finally, with SNIa from the ZTF 2018 cosmology sample, we again find a similar trend. All supernovae with excesses are on average marginally brighter than those without excesses, with  $\Delta HR = -0.128 \pm 0.046$  mag. This trend also emerges when just looking at the gold tier:  $\Delta HR = -0.327 \pm 0.102$  mag.

Taking the no-overlap weighted average of the Yao et al. (2019) and Dhawan et al. (2022) SNIa sam-

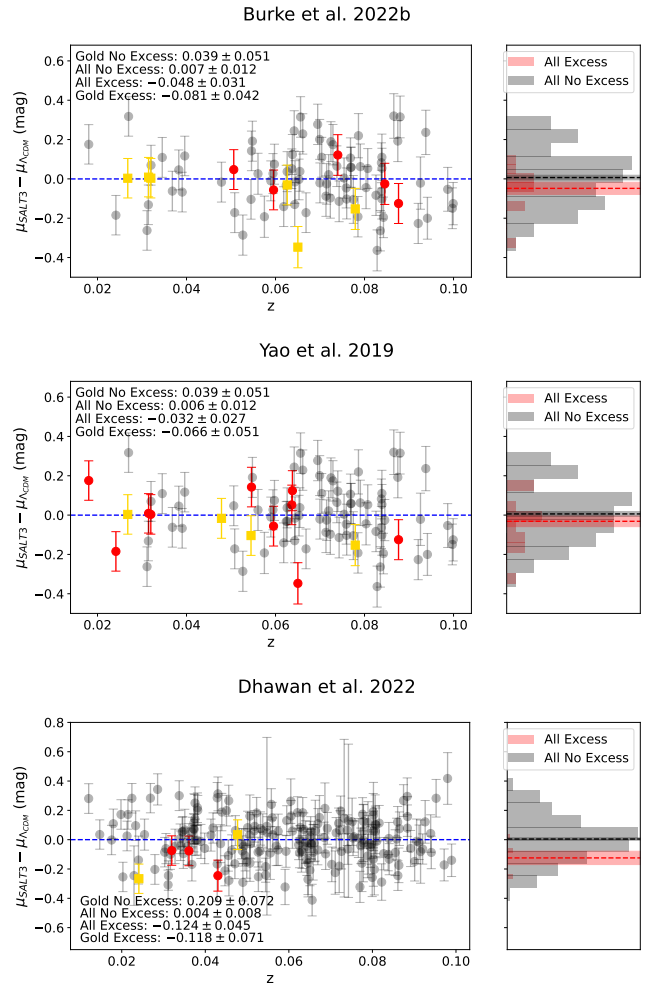


**Figure 4.** Hubble residuals for our sample. (Top): SNIa from Burke et al. (2022a), (Middle): SNIa from Yao et al. (2019), and (Bottom): SNIa from Dhawan et al. (2022). For all panels, SNIa in grey are non-excess SNIa, red are bronze excess, and gold are gold excess. The histograms to the right of each panel show the Hubble residual dispersion for all excess-having (gold + bronze) SNIa in red and excess-less (any other object) SNIa in gray; average and  $1\sigma$  intervals are shown with the shaded bars.

ples, we find that gold-tier excess-having and excess-less SNIa differ in Hubble residuals by  $\Delta HR = -0.198 \pm 0.062 = 3.2\sigma$ , and all (gold and bronze) excess-having SNIa differ from the remaining SNIa by  $\Delta HR = -0.056 \pm 0.026$  mag, or  $2.2\sigma$ . This suggests that SNIa with detected early excesses may be slightly intrinsically brighter at maximum, after shape, color, and host-galaxy mass correction, by  $\sim 0.05$ – $0.1$  mag, compared to those without excesses. We note that the  $\Delta HR$  sizes are similar when the mass step is not included, with Yao et al. (2019) slightly smaller before mass step correction and Dhawan et al. (2022) slightly larger.

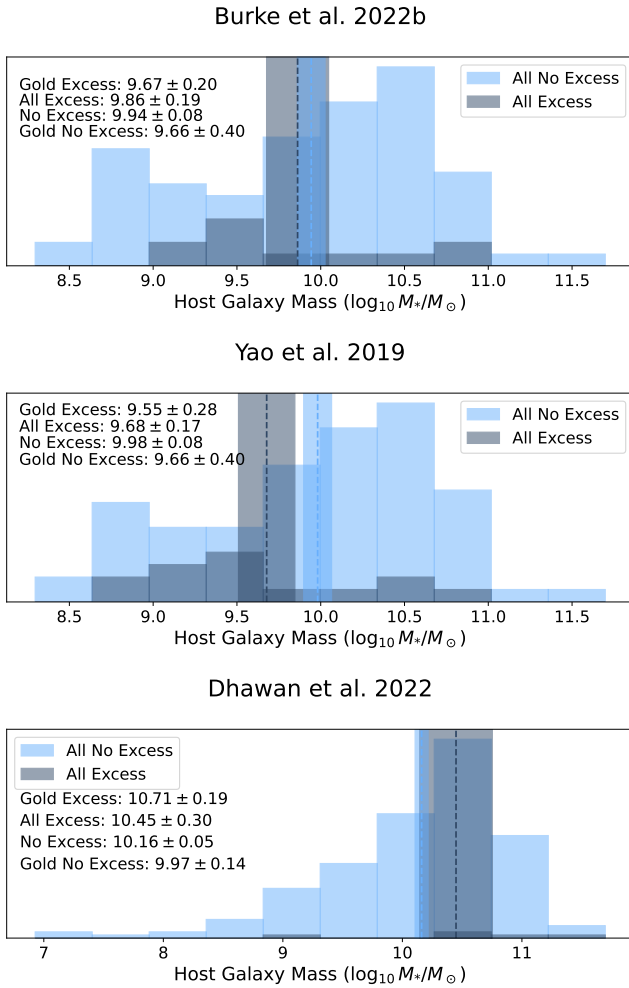


**Figure 5.** Host-galaxy masses for all excess-having (gold + bronze) and all no-excess (all other objects) SNe Ia, unscaled. Mean and  $1\sigma$  intervals are indicated in the same color scheme by dashed line and shaded vertical bars, respectively. The mass distributions of the Yao et al. (2019) data (top and middle panels) versus the Dhawan et al. (2022) sample (bottom panel) appear significantly different, perhaps due to the host-galaxy redshift cut in Dhawan et al. (2022).

#### 4.3. Host-Galaxy Masses

Many possible physical explanations for the source of early time excesses in SNe Ia — for example, single-degenerate progenitor systems (Kasen 2010) and  $^{56}\text{Ni}$  distribution (Piro & Nakar 2013) — would be expected to cause an increased early excess rate in certain host-galaxy environments given the predicted change in delay times between different SN Ia progenitor models (see Maoz et al. 2014 for a review). For that reason, we compare the stellar masses ( $\log_{10} M_*/M_\odot$ ) of matched host galaxies (see Section 2.4) for each sample. Results are shown in Figure 5.

Starting with the SNe Ia with early excesses identified in Burke et al. (2022b), we find that excess-

having supernovae, represented by the combined (gold and bronze) sample, do not exhibit any difference in host-galaxy masses as compared to excess-less (all other) SNe;  $\overline{M}_e = 9.86 \pm 0.19$  dex and  $\overline{M}_n = 9.94 \pm 0.08$  dex, with  $\overline{M}_e - \overline{M}_n = -0.08 \pm 0.21$  dex. Within the gold tier, though, we again find that SNe Ia with excesses are found in galaxies with comparable mass, with the average ( $N = 5$ )  $\log_{10} M_*/M_\odot \equiv \overline{M}_e = 9.67 \pm 0.20$  dex, compared to the average ( $N = 4$ )  $\overline{M}_n = 9.66 \pm 0.40$  dex for gold-tier excess-less SN;  $\overline{M}_e - \overline{M}_n = 0.01 \pm 0.45$  dex.

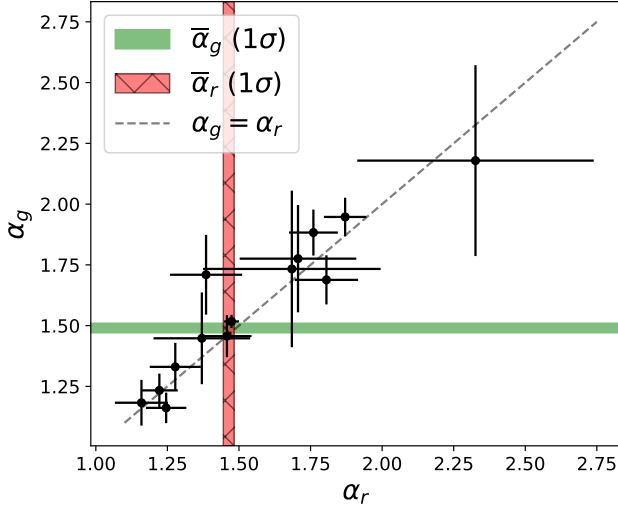
Based on the SNe Ia in Yao et al. (2019), we find that the combined sample of excess-having SNe Ia actually has a subtle preference for lower-mass galaxies, with  $\overline{M}_e = 9.68 \pm 0.17$  dex,  $\overline{M}_n = 9.98 \pm 0.08$  dex, and  $\overline{M}_e - \overline{M}_n = -0.30 \pm 0.19$  dex ( $1.6\sigma$ ). Gold-tier SNe Ia, appear to exhibit no preference for lower-mass galaxies;  $\overline{M}_e = 9.55 \pm 0.28$  dex,  $\overline{M}_n = 9.66 \pm 0.40$  dex, for a difference of  $\overline{M}_e - \overline{M}_n = -0.11 \pm 0.49$  dex.

Finally, with SNe Ia from the ZTF 2018 cosmology data release, we find that, on average, the excess-having supernovae appear in slightly higher-mass galaxies than those without excesses:  $\overline{M}_e = 10.45 \pm 0.30$  dex,  $\overline{M}_n = 10.16 \pm 0.05$  dex, and  $\overline{M}_e - \overline{M}_n = 0.29 \pm 0.30$  dex. This trend holds for the gold tier:  $\overline{M}_e = 10.71 \pm 0.19$  dex and the gold-tier excess-having sample has  $\overline{M}_e = 10.71 \pm 0.19$ , with  $\overline{M}_e - \overline{M}_n = 0.74 \pm 0.24$  dex.

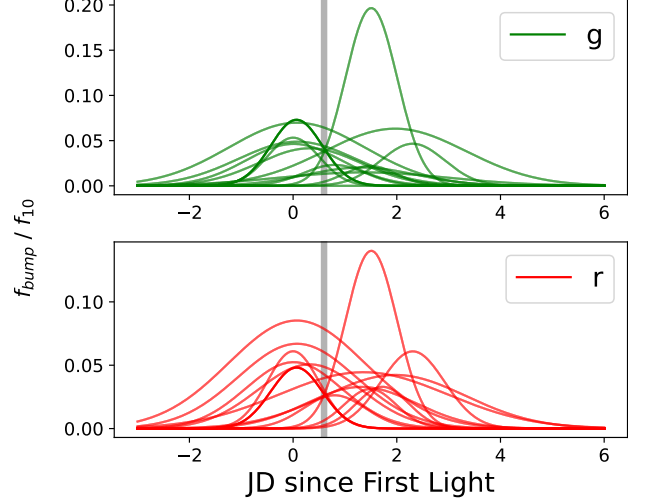
Overall, there is no clear trend between early-excess supernovae and the masses of their host galaxies. When taking the no-overlap weighted average of the Yao et al. (2019) and Dhawan et al. (2022) samples, we find that there is an insignificant average offset of  $-0.25 \pm 0.17$  dex in the host galaxy mass of SNe Ia with and without flux excesses. However, we note that because Dhawan et al. (2022) only uses samples with measured host-galaxy redshifts, there is a significant bias in the host-galaxy masses of this sample. While we wouldn't necessarily expect this selection to change the relative difference in host-galaxy mass between the excess-having and no-excess populations, the Yao et al. (2019) sample is less biased as a function of host mass and has better sample statistics.

#### 4.4. Light-curve Properties

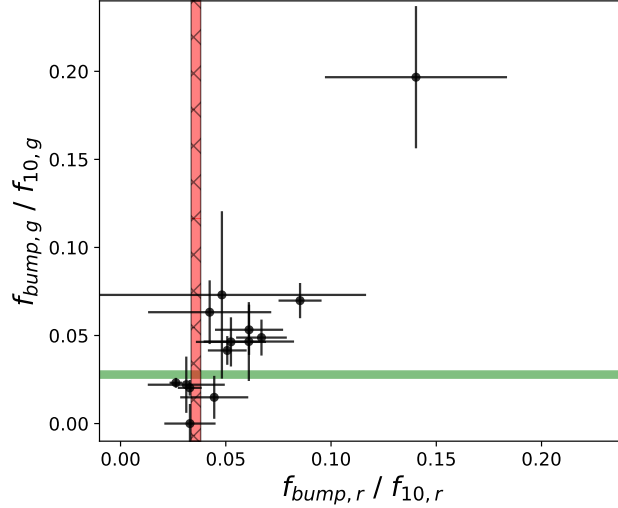
Finally, we analyze the statistical properties of the light curves of early-excess SNe Ia from the Yao et al. (2019) sample (see Figure 6). All averages quoted in this section are weighted by the uncertainties. Based on a fireball model (Riess et al. 1999), we expect the first few days post-explosion to be well-fit by a power law, approximately  $t^2$ , but previous studies have found a diversity of power-law slopes (Miller et al. 2020; Fausnaugh et al. 2021). Among 14 total SNe Ia with early excesses,



(a) Power-law slopes,  $\alpha$ , in ZTF  $g$  and  $r$  bands. Green and red bars span the  $1\sigma$  uncertainty on the mean for  $g$  and  $r$  band, respectively.



(b) Traces of relative excess sizes, scaled by 10-day flux, in  $g$  and  $r$  bands. The gray bar spans the  $1\sigma$  uncertainty on the mean.



(c) Relative excess sizes in  $g$  and  $r$  bands. Green and red bars span the  $1\sigma$  uncertainty on the mean for  $g$  and  $r$  band, respectively.

**Figure 6.** Properties of light curves from Yao et al. (2019) with early excesses.  $1\sigma$  uncertainty regions are shaded.

we find  $\alpha_r = 1.46 \pm 0.02$  and  $\alpha_g = 1.49 \pm 0.02$ , consistent with individual SNe Ia from Miller et al. (2020) but inconsistent with their population average ( $2.01 \pm 0.02$  in the  $r$  band), indicating that the rise rates may be less steep for early excess SNe. A different slope as a function of filter would be expected for a changing SED temperature, but here we find that  $g$ -band rises are consistent with  $r$ -band rises with a difference of  $0.03 \pm 0.03$ .

While many physical models of early excesses predict stronger excesses at bluer wavelengths, we do not find a significant color dependence. Excess-having SNe Ia from the literature also have a range of colors, though many of the earliest known examples were blue: 2017cbv had

a  $g - r$  color of approximately  $-0.2$  mag (Hosseinzadeh et al. 2017), as did 2018oh (Dimitriadis et al. 2019, albeit very uncertain). SN 2012cg had  $B - V \simeq -0.1$  mag in its earliest epoch. Here, we see a wider range of colors; for example, we find an exclusively red excess in ZTF18aaxsioa and an average  $g - r = 0.06 \pm 0.09$  mag for the other 13 SNe Ia. Other studies of ZTF SNe have found similar results, with Deckers et al. (2022) have  $g - r$  colors spanning from  $-0.35$  to  $+0.15$  mag, though with an average of  $-0.14$  mag (uncertainties range from  $\sim 0.1$ – $0.6$  mag). Similarly, Burke et al. (2022a) saw that ZTF SNe with early excesses often have redder early

time colors (Burke et al. 2022b also saw this in a literature sample using  $B - V$  colors).

Averaged among all Yao et al. (2019) SNe Ia with detections, the early excess flux has mean absolute magnitudes of  $M_g = -15.55 \pm 0.33$  and  $M_r = -15.72 \pm 0.25$ . Within our (rather restrictive) priors, we find that the average early excess peaks at  $0.60 \pm 0.05$  days after explosion, and has a Gaussian standard deviation of  $\sigma = 0.71 \pm 0.02$  days.

## 5. DISCUSSION

### 5.1. *Robustly Identifying Early Excess SNe Ia*

The task of systematically selecting early excess SNe Ia is a difficult one, due to non-uniformity in both the input light curves and the diverse nature of the early excesses. We found in this work that the detection of early excesses can be degenerate with the slope of the power-law rise and the time of explosion (Figure 3). Lack of sufficient sampling immediately post-explosion, outliers in the light curves, and occasional under-estimated uncertainties added additional complexity. Because early excess detections are often subtle, we found that detecting them is not always unambiguous; we did not confidently find excesses for several objects with early excesses reported in the literature. In this study, following Burke et al. (2022a), we felt this necessitated including different tiers of confidence for how reliable the detections were and several criteria to account for uncertainties in the fitting and data. While future data will inevitably increase the statistics for early excess studies, we expect that high-cadence survey or follow-up data will be particularly valuable for robust detections.

### 5.2. *Subsample Comparison and Future Improvements*

While the Dhawan et al. (2022) data were intended to be used for cosmological analyses, the ZTF forced-photometry data from Yao et al. (2019) were not. Despite this, the light-curve calibration appears to be sufficient to yield a Hubble-diagram scatter that is competitive with other recent cosmology samples, including Dhawan et al. (2022).

We note that we found two differences between the Yao et al. (2019) and Dhawan et al. (2022) samples in our distance fitting. The first is that the  $\beta$  parameter relating color to distance modulus is different at just under  $3\sigma$  significance between the two samples (Table 1). This difference could be related to either sample selection effects or uncorrected calibration uncertainties in the 2018 ZTF photometry.

We note that both subsamples were derived with different photometric pipelines. While the Yao et al. (2019)

used the difference images from IPAC (e.g., see Masci et al. 2019) and PSF photometry with ForcedPhotZTF, Dhawan et al. (2022) construct custom template images and difference images and then used photutils (Bradley et al. 2023) for performing forced photometry. Given these differences in the processing, we do not combine the photometric data, instead analyzing each self-consistent sample independently and using weighted averages to yield final constraints.

Secondly, the distance bias significantly differs between Yao et al. (2019)-derived distances and those of Dhawan et al. (2022). This is likely due to sample selection; while Dhawan et al. (2022) started with a magnitude-limited sample and made additional cuts on host-galaxy redshift availability (thereby favoring bright host galaxies), Yao et al. (2019) selected their sample based on the availability of high-S/N, high-cadence early-time light curves. We attempt to marginalize over these differences by fitting a model to the redshift-dependent Hubble residuals and correcting for the trends, which are substantially different between the two data sets in this work. This procedure is standard practice for SN Ia cosmology (e.g., Marriner et al. 2011), but cosmology analyses also typically use large Monte Carlo simulations to estimate and correct for distance bias, which we have not performed here because it is not necessary for us to separate redshift-dependent Malmquist biases from differences in the cosmological model. More complex evaluations of the distance bias will likely be performed by the ZTF team in the future, which could include pixel-level pipelines to model search/classification efficiencies and perform scene-modeling photometry.

Despite those caveats, our methodology avoided most major sources of systematic uncertainty by performing self-consistent comparisons between excess-having and no-excess SNe Ia within each individual data set. Higher-dimensional models of selection effects (i.e., correcting for  $x_1$  and  $c$  measurement biases; Kessler & Scolnic 2017) would be unlikely to substantially change the results given the high-S/N ZTF data and the similar average values of  $x_1$  and  $c$  between the samples. We consider it more likely than not that SN Ia distance measurements do correlate with behavior in the early time light curves of SNe Ia, and we anticipate future work on this topic with larger, better-calibrated, cosmologically useful SNe Ia samples such as future ZTF data releases.

### 5.3. *Possible Impact on Measurements of Dark Energy Properties*

Although early-excess SNe Ia are a minority of the SN Ia sample, it is possible that they comprise a larger



$\Delta\text{HR}$ (mag)	$\Delta f_e$ (%)	$\mu$ bias (mag)	$\Delta w$ ( $z = 1$ )
0.05	5	0.003	0.007
0.05	10	0.005	0.013
0.05	15	0.007	0.020
0.10	5	0.005	0.013
0.10	10	0.010	0.027
0.10	15	0.015	0.041
0.15	5	0.007	0.020
0.15	10	0.015	0.041
0.15	15	0.022	0.062

**Table 5.** Biases on  $w$  inferred from comparing a  $z = 1$  SN Ia sample to a  $z = 0.05$  sample as a function of different Hubble residual steps due to early excesses ( $\Delta\text{HR}$ ) and changes in early excess fraction between  $z = 0$  and  $z = 1$  ( $\Delta f_e$ ). The product of the first and second columns is the average bias on distance at  $z = 1$  ( $\mu$  bias).

fraction of high-redshift samples. Here, we see hints that they might be more prevalent in low-mass galaxies, which are likely those with younger stellar populations. Additionally, if they are indeed slightly brighter, surveys are more likely to detect them near the high- $z$  magnitude limit.

As a back-of-the-envelope example, in the Pantheon+ sample (Scolnic et al. 2022), 58% of the SNe Ia at  $z < 0.1$  but just 25% of SNe Ia at  $z > 0.8$  have host-galaxy masses greater than 10 dex. Early excesses from Yao et al. (2019) are present in  $\sim 9\%$  of the mass  $> 10$  dex SN Ia sample, but 23% of the  $< 10$  dex sample; this equates to 15% of the full low- $z$  sample and 20% of the  $z > 0.8$  sample. If early excess SNe Ia have 10% brighter Hubble residuals, this could imply a systematic offset in the distances of  $\sim 0.5\%$  between high- and low-redshift SNe. Such an offset could introduce 1-2% biases on the dark energy equation of state parameter,  $w$ , which would be a dominant systematic in current  $w$  measurements (Brout et al. 2022). Table 5 demonstrates how changes in excess fraction with redshift and different values of  $\Delta\text{HR}$  (chosen to be consistent with our results) would naively translate to biases on  $w$  for a  $z = 1$  SN Ia sample.

This rough calculation highlights the importance of investigating these potential changes in the SN Ia population over cosmic time. It is not intended as a definitive assessment of what biases might exist, and it assumes that the early excess rate as a function of host mass is fixed – likely a poor assumption. For example, the SN Ia rate as a function of host-galaxy mass (Brown et al. 2019; Wiseman et al. 2021) appears to increase in low-metallicity environments due to an increased binary fraction (Gandhi et al. 2022; Johnson et al. 2023),

which could affect e.g., single-degenerate progenitors to a different degree than double-degenerate progenitors. It is also not necessary to observe early excesses at high redshift to correct for this bias; for example, a redshift-binned host-galaxy mass correction, would likely correct for this type of systematic distance offset (use of twin or sibling SNe — SNe with similar spectra or in similar host-galaxy types — could be another option; e.g., Fakhouri et al. 2015; Hoogendam et al. 2023). However, current analyses do not make such corrections, and without *a priori* knowledge of what systematics could be problematic, these types of cosmological biases could be neglected.

## 6. CONCLUSIONS

In this work, we search for a change in Hubble residuals between SNe Ia with and without flux excesses in their early-time light curves. Although there is no consensus physical explanation for why a minority of SNe Ia have rises that are not well represented by a single power-law model, we hypothesize that such behavior could be correlated with intrinsic SN Ia luminosity differences that propagate to distance measurements.

By examining two samples of ZTF SNe Ia with well-sampled early time light curves, we find 17 SNe Ia with significant detected excesses. These SNe Ia have modest evidence for brighter Hubble residuals,  $\Delta\text{HR} = -0.056 \pm 0.026$  mag ( $2.2\sigma$  significance), compared to the rest of the sample. SNe Ia with early excesses are found more often in lower-mass host galaxies, though the statistical significance is low, and host-galaxy selection effects are inherent in one of our samples. Our detected excesses have an average  $g - r$  color of  $0.06 \pm 0.09$  mag. We also find that excess-having SNe Ia rise less quickly than the mean Yao et al. (2019) SN Ia as measured by Miller et al. (2020).

This work highlights the importance of connecting new diagnostics of SN Ia physics to cosmological parameter measurements. Fortunately for the current study, future data releases from ZTF and ATLAS (Tonry et al. 2018), alongside hundreds of thousands of SN Ia discoveries from the Rubin Observatory, will give a clear indication of the degree to which early time excesses correlate with distance measurements. However, future surveys such as the *Roman Space Telescope* will observe SNe Ia at unprecedented redshifts ( $z > 2$ ) to measure dark energy, and therefore require a comprehensive understanding of the ways that SN Ia distance measurements could become biased as their progenitors evolve with cosmic time.

*Software:* Astropy (Astropy Collaboration et al. 2013, 2018), sncosmo (Barbary et al. 2022), GHOST



(Gagliano et al. 2021), `dustmaps` (Green 2018), `SciPy` (Virtanen et al. 2020), `matplotlib` (Hunter 2007), `NumPy` (Harris et al. 2020), `PyMultiNest` (Buchner et al. 2014), `corner` (Foreman-Mackey 2016)

1 C.Y. and D.O.J acknowledge support from *HST* grants  
 2 HST-GO-17128.028 and HST-GO-16269.012 awarded  
 3 by the Space Telescope Science Institute (STScI), which  
 4 is operated by the Association of Universities for Re-  
 5 search in Astronomy, Inc., for NASA, under contract  
 6 NAS5-26555.

## APPENDIX

### A. EARLY-EXCESS CRITERIA

Here, we list the specific criteria for our “gold” and “bronze” detections of early excesses, as well as our “gold” non-detections. An overview of how these samples are used in our analysis is given in Section 3.2. In addition to the criteria below, each light curve has been inspected visually as an additional check on the fidelity of the model fit and data quality. Our fits to “gold” and “bronze” light curves are shown in Figures 1, 7 and 8.

The gold excess-having sample is defined as follows:

1. The SNIa has at least 2 data points between  $-5$  and 0 days prior to  $t_{exp}$ .
2. For at least 2 consecutive values of  $N$  (the maximum epoch used for PL fitting), the BIC for the Gaussian+PL model is at least 5 less than the BIC for the PL-only model.
3. At least two consecutive data points in a single band favor the Gaussian+PL model over the PL-only model at  $> 3\sigma$  significance.
4. The reduced  $\chi^2$  of the fit is  $< 3$ .
5. Data for at least 2 epochs exist within  $2\sigma$  of the best-measured excess (i.e., in  $[\mu - 2\sigma, \mu + 2\sigma]$ ).
6. There are no  $> 10\sigma$  outliers in the full model fit.
7. The amplitude of the Gaussian component has at least  $3\sigma$  significance and there are no nearby outliers of comparable significance to the detected Gaussian component.
8. In at least one band, the bump amplitude is at least 2% of the 10-day post-explosion flux.
9. An excess is still detected even if a stricter ( $[1.75, 2.25]$ ) prior on the PL slope  $\alpha$  is enforced.

The bronze excess-having sample is defined similarly, with relaxed criteria:

1. The SNIa has at least one pre-explosion data point.

2. Either at least 2 data points are  $> 3\sigma$  different between the full Gaussian+PL fit and the fit with Gaussian subtracted *or* the BIC prefers the Gaussian+PL model and at least one data point is  $> 3\sigma$  different between the Gaussian+PL fit and the Gaussian-subtracted fit.
3. The reduced  $\chi^2$  of the fit is  $< 6$ .
4. Data for at least one epoch exists within  $2\sigma$  of the best-measured excess (i.e., in  $[\mu - 2\sigma, \mu + 2\sigma]$ ).
5. The SNIa has  $\leq 1$  extreme,  $> 10\sigma$  outliers in the full model fit.
6. The “bump” amplitude is at least 1% of the 10-day post-explosion flux in at least one band.
7. There are no nearby outliers of comparable significance to the detected Gaussian component.

Finally, we define a gold tier for no-excess SNe:

1. Has at least 2 data points pre-explosion (between  $-5$  and 0 days).
2. The BIC for the Gaussian+PL model is greater than the BIC for the PL-only model.
3. There are no significant ( $3\sigma$ ) differences in any data point between the Gaussian+PL model and the same model after the Gaussian component has been subtracted.
4. The reduced  $\chi^2$  of the fit is  $< 3$ .
5. The SNIa has at least 2 data points between  $t_{exp}$  and  $t_{exp} + 5$  (the time range when we would expect an early excess to occur) in each band.
6. There are no extreme ( $> 10\sigma$ ) outliers in the full model fit.
7. The amplitude of the Gaussian component is  $< 2\sigma$  significant and less than 2% of the 10-day post-explosion flux in both bands.

8. There are no claims of an early excess in the literature (e.g., Yao et al. 2019; Bulla et al. 2020;

Miller et al. 2020; Deckers et al. 2022; Burke et al. 2022a).

## REFERENCES

- Ashall, C., Hoeflich, P., Hsiao, E. Y., et al. 2019, *ApJ*, 878, 86, doi: [10.3847/1538-4357/ab204b](https://doi.org/10.3847/1538-4357/ab204b)
- Ashall, C., Lu, J., Shappee, B. J., et al. 2022, *ApJL*, 932, L2, doi: [10.3847/2041-8213/ac7235](https://doi.org/10.3847/2041-8213/ac7235)
- Astropy Collaboration, Robitaille, T. P., Tollerud, E. J., et al. 2013, *A&A*, 558, A33, doi: [10.1051/0004-6361/201322068](https://doi.org/10.1051/0004-6361/201322068)
- Astropy Collaboration, Price-Whelan, A. M., Sipőcz, B. M., et al. 2018, *AJ*, 156, 123, doi: [10.3847/1538-3881/aabc4f](https://doi.org/10.3847/1538-3881/aabc4f)
- Barbary, K., Bailey, S., Barentsen, G., et al. 2022, *SNCosmo*, v2.8.0, Zenodo, Zenodo, doi: [10.5281/zenodo.6363879](https://doi.org/10.5281/zenodo.6363879)
- Bellm, E. C., Kulkarni, S. R., Graham, M. J., et al. 2019, *PASP*, 131, 018002, doi: [10.1088/1538-3873/aaecbe](https://doi.org/10.1088/1538-3873/aaecbe)
- Betoule, M., Kessler, R., Guy, J., et al. 2014, *A&A*, 568, A22, doi: [10.1051/0004-6361/201423413](https://doi.org/10.1051/0004-6361/201423413)
- Bradley, L., Sipőcz, B., Robitaille, T., et al. 2023, *astropy/photutils*: 1.8.0, 1.8.0, Zenodo, doi: [10.5281/zenodo.7946442](https://doi.org/10.5281/zenodo.7946442)
- Brout, D., & Scolnic, D. 2021, *ApJ*, 909, 26, doi: [10.3847/1538-4357/abd69b](https://doi.org/10.3847/1538-4357/abd69b)
- Brout, D., Scolnic, D., Popovic, B., et al. 2022, arXiv e-prints, arXiv:2202.04077, <https://arxiv.org/abs/2202.04077>
- Brown, J. S., Stanek, K. Z., Holoién, T. W. S., et al. 2019, *MNRAS*, 484, 3785, doi: [10.1093/mnras/stz258](https://doi.org/10.1093/mnras/stz258)
- Buchner, J., Georgakakis, A., Nandra, K., et al. 2014, *A&A*, 564, A125, doi: [10.1051/0004-6361/201322971](https://doi.org/10.1051/0004-6361/201322971)
- Bulla, M., Miller, A. A., Yao, Y., et al. 2020, *ApJ*, 902, 48, doi: [10.3847/1538-4357/abb13c](https://doi.org/10.3847/1538-4357/abb13c)
- Burke, J., Howell, D. A., Sand, D. J., & Hosseinzadeh, G. 2022a, arXiv e-prints, arXiv:2208.11201, doi: [10.48550/arXiv.2208.11201](https://doi.org/10.48550/arXiv.2208.11201)
- Burke, J., Howell, D. A., Sand, D. J., et al. 2022b, arXiv e-prints, arXiv:2207.07681, doi: [10.48550/arXiv.2207.07681](https://doi.org/10.48550/arXiv.2207.07681)
- Burns, C. R., Parent, E., Phillips, M. M., et al. 2018, *ApJ*, 869, 56, doi: [10.3847/1538-4357/aae51c](https://doi.org/10.3847/1538-4357/aae51c)
- Carrick, J., Turnbull, S. J., Lavaux, G., & Hudson, M. J. 2015, *MNRAS*, 450, 317, doi: [10.1093/mnras/stv547](https://doi.org/10.1093/mnras/stv547)
- Childress, M. J., Wolf, C., & Zahid, H. J. 2014, *MNRAS*, 445, 1898, doi: [10.1093/mnras/stu1892](https://doi.org/10.1093/mnras/stu1892)
- Contreras, C., Phillips, M. M., Burns, C. R., et al. 2018, *ApJ*, 859, 24, doi: [10.3847/1538-4357/aabaf8](https://doi.org/10.3847/1538-4357/aabaf8)
- Deckers, M., Maguire, K., Magee, M. R., et al. 2022, *MNRAS*, 512, 1317, doi: [10.1093/mnras/stac558](https://doi.org/10.1093/mnras/stac558)
- Desai, D. D., Kochanek, C. S., Shappee, B. J., et al. 2023, arXiv e-prints, arXiv:2306.11100, doi: [10.48550/arXiv.2306.11100](https://doi.org/10.48550/arXiv.2306.11100)
- Dhawan, S., Brout, D., Scolnic, D., et al. 2020, *ApJ*, 894, 54, doi: [10.3847/1538-4357/ab7fb0](https://doi.org/10.3847/1538-4357/ab7fb0)
- Dhawan, S., Thorp, S., Mandel, K. S., et al. 2023, *MNRAS*, 524, 235, doi: [10.1093/mnras/stad1590](https://doi.org/10.1093/mnras/stad1590)
- Dhawan, S., Goobar, A., Smith, M., et al. 2022, *MNRAS*, 510, 2228, doi: [10.1093/mnras/stab3093](https://doi.org/10.1093/mnras/stab3093)
- Di Valentino, E., Mena, O., Pan, S., et al. 2021, *Classical and Quantum Gravity*, 38, 153001, doi: [10.1088/1361-6382/ac086d](https://doi.org/10.1088/1361-6382/ac086d)
- Diamond, T. R., Hoeflich, P., Hsiao, E. Y., et al. 2018, *ApJ*, 861, 119, doi: [10.3847/1538-4357/aac434](https://doi.org/10.3847/1538-4357/aac434)
- Dimitriadis, G., Foley, R. J., Rest, A., et al. 2019, *ApJL*, 870, L1, doi: [10.3847/2041-8213/aaedb0](https://doi.org/10.3847/2041-8213/aaedb0)
- Dimitriadis, G., Maguire, K., Karambelkar, V. R., et al. 2023, *MNRAS*, 521, 1162, doi: [10.1093/mnras/stad536](https://doi.org/10.1093/mnras/stad536)
- Domínguez, I., Höflich, P., & Straniero, O. 2001, *ApJ*, 557, 279, doi: [10.1086/321661](https://doi.org/10.1086/321661)
- Fakhouri, H. K., Boone, K., Aldering, G., et al. 2015, *ApJ*, 815, 58, doi: [10.1088/0004-637X/815/1/58](https://doi.org/10.1088/0004-637X/815/1/58)
- Fausnaugh, M. M., Valley, P. J., Kochanek, C. S., et al. 2021, *ApJ*, 908, 51, doi: [10.3847/1538-4357/abcd42](https://doi.org/10.3847/1538-4357/abcd42)
- Fausnaugh, M. M., Valley, P. J., Tucker, M. A., et al. 2023, arXiv e-prints, arXiv:2307.11815, doi: [10.48550/arXiv.2307.11815](https://doi.org/10.48550/arXiv.2307.11815)
- Fink, M., Hillebrandt, W., & Röpke, F. K. 2007, *A&A*, 476, 1133, doi: [10.1051/0004-6361:20078438](https://doi.org/10.1051/0004-6361:20078438)
- Flewelling, H. A., Magnier, E. A., Chambers, K. C., et al. 2020, *ApJS*, 251, 7, doi: [10.3847/1538-4365/abb82d](https://doi.org/10.3847/1538-4365/abb82d)
- Foreman-Mackey, D. 2016, *The Journal of Open Source Software*, 1, 24, doi: [10.21105/joss.00024](https://doi.org/10.21105/joss.00024)
- Freedman, W. L., Madore, B. F., Hatt, D., et al. 2019, *ApJ*, 882, 34, doi: [10.3847/1538-4357/ab2f73](https://doi.org/10.3847/1538-4357/ab2f73)
- Gagliano, A., Narayan, G., Engel, A., Carrasco Kind, M., & LSST Dark Energy Science Collaboration. 2021, *ApJ*, 908, 170, doi: [10.3847/1538-4357/abd02b](https://doi.org/10.3847/1538-4357/abd02b)
- Gandhi, P. J., Wetzell, A., Hopkins, P. F., et al. 2022, *MNRAS*, 516, 1941, doi: [10.1093/mnras/stac2228](https://doi.org/10.1093/mnras/stac2228)
- Garnavich, P., Wood, C. M., Milne, P., et al. 2023, *ApJ*, 953, 35, doi: [10.3847/1538-4357/ace04b](https://doi.org/10.3847/1538-4357/ace04b)

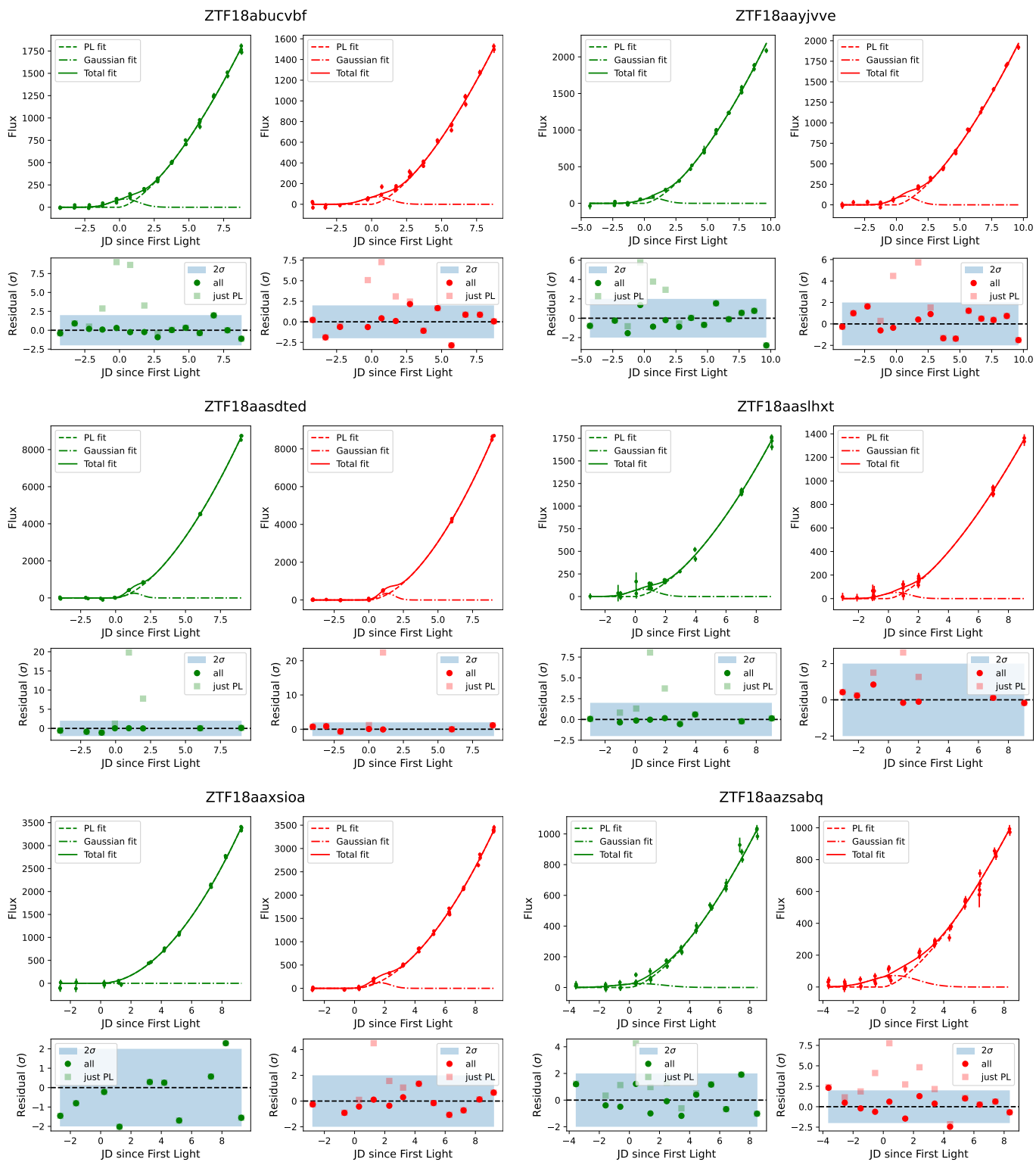


Figure 7. Other early-excess SNe Ia from Yao et al. (2019).

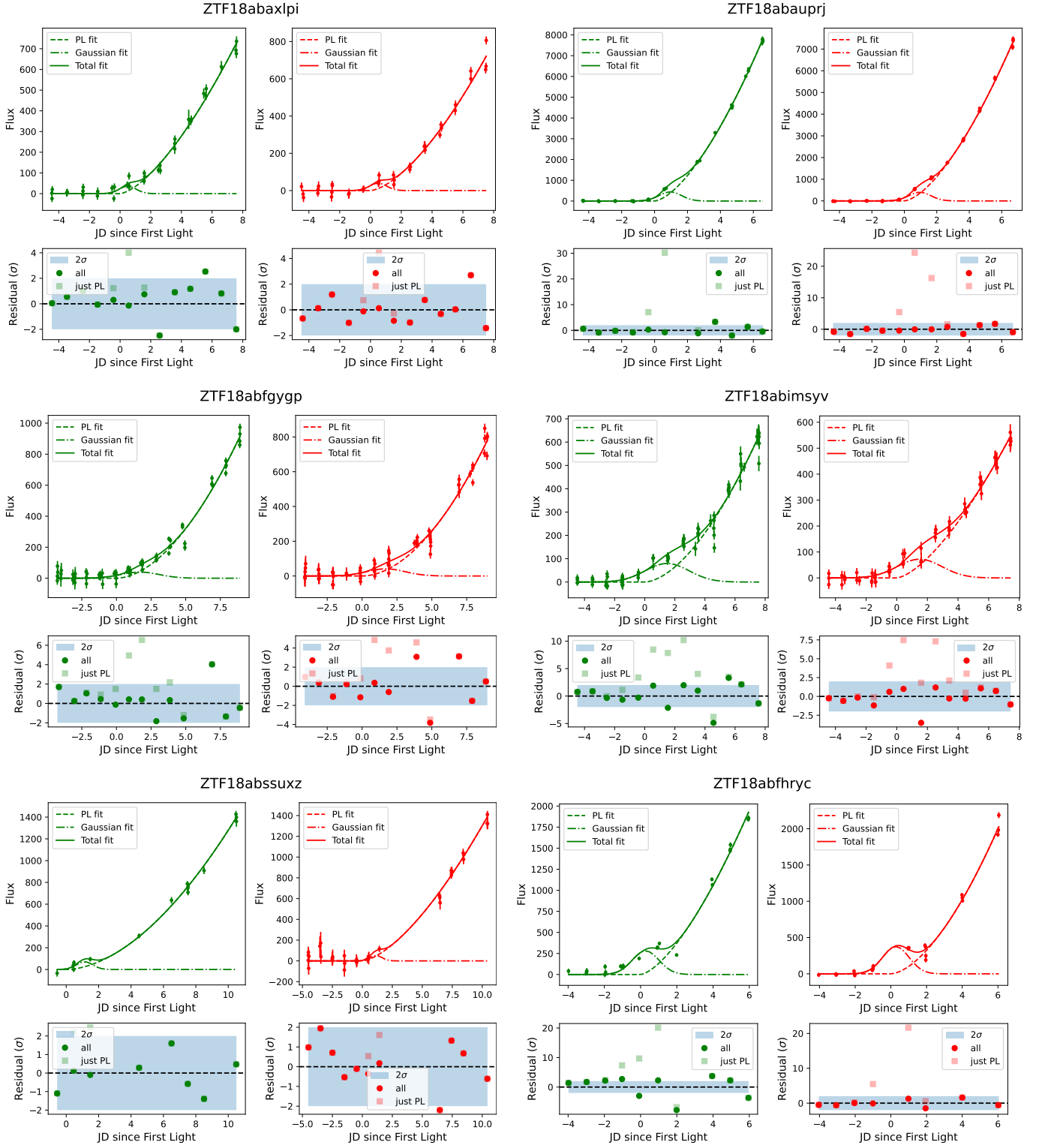


Figure 8. Other early-excess SNe Ia from Yao et al. (2019), contd.

- Goobar, A., Kromer, M., Siverd, R., et al. 2015, *ApJ*, 799, 106, doi: [10.1088/0004-637X/799/1/106](https://doi.org/10.1088/0004-637X/799/1/106)
- Green, G. 2018, *The Journal of Open Source Software*, 3, 695, doi: [10.21105/joss.00695](https://doi.org/10.21105/joss.00695)
- Guy, J., Astier, P., Nobili, S., Regnault, N., & Pain, R. 2005, *A&A*, 443, 781, doi: [10.1051/0004-6361:20053025](https://doi.org/10.1051/0004-6361:20053025)
- Guy, J., Astier, P., Baumont, S., et al. 2007, *A&A*, 466, 11, doi: [10.1051/0004-6361:20066930](https://doi.org/10.1051/0004-6361:20066930)
- Harris, C. R., Millman, K. J., van der Walt, S. J., et al. 2020, *Nature*, 585, 357, doi: [10.1038/s41586-020-2649-2](https://doi.org/10.1038/s41586-020-2649-2)
- Hoeflich, P., & Khokhlov, A. 1996, *ApJ*, 457, 500, doi: [10.1086/176748](https://doi.org/10.1086/176748)
- Hoogendam, W. B., Shappee, B. J., Brown, P. J., et al. 2023, arXiv e-prints, arXiv:2309.11563, doi: [10.48550/arXiv.2309.11563](https://doi.org/10.48550/arXiv.2309.11563)
- Hosseinzadeh, G., Sand, D. J., Valenti, S., et al. 2017, *ApJL*, 845, L11, doi: [10.3847/2041-8213/aa8402](https://doi.org/10.3847/2041-8213/aa8402)
- Hosseinzadeh, G., Sand, D. J., Lundqvist, P., et al. 2022, *ApJL*, 933, L45, doi: [10.3847/2041-8213/ac7cef](https://doi.org/10.3847/2041-8213/ac7cef)
- Hosseinzadeh, G., Sand, D. J., Sarbadhicary, S. K., et al. 2023, arXiv e-prints, arXiv:2305.03071, doi: [10.48550/arXiv.2305.03071](https://doi.org/10.48550/arXiv.2305.03071)
- Hoyle, F., & Fowler, W. A. 1960, *ApJ*, 132, 565, doi: [10.1086/146963](https://doi.org/10.1086/146963)
- Hunter, J. D. 2007, *Computing in Science and Engineering*, 9, 90, doi: [10.1109/MCSE.2007.55](https://doi.org/10.1109/MCSE.2007.55)
- Iben, I. J., & Tutukov, A. V. 1984, *ApJS*, 54, 335, doi: [10.1086/190932](https://doi.org/10.1086/190932)
- Jha, S. W., Maguire, K., & Sullivan, M. 2019, *Nature Astronomy*, 3, 706, doi: [10.1038/s41550-019-0858-0](https://doi.org/10.1038/s41550-019-0858-0)
- Jiang, J.-a., Doi, M., Maeda, K., & Shigeyama, T. 2018, *ApJ*, 865, 149, doi: [10.3847/1538-4357/aadb9a](https://doi.org/10.3847/1538-4357/aadb9a)
- Jiang, J.-A., Doi, M., Maeda, K., et al. 2017, *Nature*, 550, 80, doi: [10.1038/nature23908](https://doi.org/10.1038/nature23908)
- Jiang, J.-a., Maeda, K., Kawabata, M., et al. 2021, *ApJL*, 923, L8, doi: [10.3847/2041-8213/ac375f](https://doi.org/10.3847/2041-8213/ac375f)
- Johnson, J. W., Kochanek, C. S., & Stanek, K. Z. 2023, *MNRAS*, 526, 5911, doi: [10.1093/mnras/stad3019](https://doi.org/10.1093/mnras/stad3019)
- Jones, D. O., Scolnic, D. M., Riess, A. G., et al. 2018, *ApJ*, 857, 51, doi: [10.3847/1538-4357/aab6b1](https://doi.org/10.3847/1538-4357/aab6b1)
- Jones, D. O., Scolnic, D. M., Foley, R. J., et al. 2019, *ApJ*, 881, 19, doi: [10.3847/1538-4357/ab2bec](https://doi.org/10.3847/1538-4357/ab2bec)
- Jönsson, J., Sullivan, M., Hook, I., et al. 2010, *MNRAS*, 405, 535, doi: [10.1111/j.1365-2966.2010.16467.x](https://doi.org/10.1111/j.1365-2966.2010.16467.x)
- Kasen, D. 2010, *ApJ*, 708, 1025, doi: [10.1088/0004-637X/708/2/1025](https://doi.org/10.1088/0004-637X/708/2/1025)
- Kelly, P. L., Hicken, M., Burke, D. L., Mandel, K. S., & Kirshner, R. P. 2010, *ApJ*, 715, 743, doi: [10.1088/0004-637X/715/2/743](https://doi.org/10.1088/0004-637X/715/2/743)
- Kelsey, L., Sullivan, M., Wiseman, P., et al. 2022, arXiv e-prints, arXiv:2208.01357, <https://arxiv.org/abs/2208.01357>
- . 2023, *MNRAS*, 519, 3046, doi: [10.1093/mnras/stac3711](https://doi.org/10.1093/mnras/stac3711)
- Kenworthy, W. D., Jones, D. O., Dai, M., et al. 2021, *ApJ*, 923, 265, doi: [10.3847/1538-4357/ac30d8](https://doi.org/10.3847/1538-4357/ac30d8)
- Kessler, R., & Scolnic, D. 2017, *ApJ*, 836, 56, doi: [10.3847/1538-4357/836/1/56](https://doi.org/10.3847/1538-4357/836/1/56)
- Kromer, M., Fremling, C., Pakmor, R., et al. 2016, *MNRAS*, 459, 4428, doi: [10.1093/mnras/stw962](https://doi.org/10.1093/mnras/stw962)
- Kumar, S., Hsiao, E. Y., Ashall, C., et al. 2023, *ApJ*, 945, 27, doi: [10.3847/1538-4357/acad73](https://doi.org/10.3847/1538-4357/acad73)
- Lampeitl, H., Smith, M., Nichol, R. C., et al. 2010, *ApJ*, 722, 566, doi: [10.1088/0004-637X/722/1/566](https://doi.org/10.1088/0004-637X/722/1/566)
- Li, W., Wang, X., Vinkó, J., et al. 2019, *ApJ*, 870, 12, doi: [10.3847/1538-4357/aaec74](https://doi.org/10.3847/1538-4357/aaec74)
- Livio, M., & Mazzali, P. 2018, *PhR*, 736, 1, doi: [10.1016/j.physrep.2018.02.002](https://doi.org/10.1016/j.physrep.2018.02.002)
- Livne, E. 1990, *ApJL*, 354, L53, doi: [10.1086/185721](https://doi.org/10.1086/185721)
- Maeda, K., Jiang, J.-a., Shigeyama, T., & Doi, M. 2018, *ApJ*, 861, 78, doi: [10.3847/1538-4357/aac8d8](https://doi.org/10.3847/1538-4357/aac8d8)
- Maeda, K., & Terada, Y. 2016, *International Journal of Modern Physics D*, 25, 1630024, doi: [10.1142/S021827181630024X](https://doi.org/10.1142/S021827181630024X)
- Magee, M. R., & Maguire, K. 2020, *A&A*, 642, A189, doi: [10.1051/0004-6361/202037870](https://doi.org/10.1051/0004-6361/202037870)
- Magee, M. R., Maguire, K., Kotak, R., et al. 2020, *A&A*, 634, A37, doi: [10.1051/0004-6361/201936684](https://doi.org/10.1051/0004-6361/201936684)
- Maoz, D., Mannucci, F., & Nelemans, G. 2014, *ARA&A*, 52, 107, doi: [10.1146/annurev-astro-082812-141031](https://doi.org/10.1146/annurev-astro-082812-141031)
- Marietta, E., Burrows, A., & Fryxell, B. 2000, *ApJS*, 128, 615, doi: [10.1086/313392](https://doi.org/10.1086/313392)
- Marion, G. H., Brown, P. J., Vinkó, J., et al. 2016, *ApJ*, 820, 92, doi: [10.3847/0004-637X/820/2/92](https://doi.org/10.3847/0004-637X/820/2/92)
- Marriner, J., Bernstein, J. P., Kessler, R., et al. 2011, *ApJ*, 740, 72, doi: [10.1088/0004-637X/740/2/72](https://doi.org/10.1088/0004-637X/740/2/72)
- Masci, F. J., Laher, R. R., Rusholme, B., et al. 2019, *PASP*, 131, 018003, doi: [10.1088/1538-3873/aae8ac](https://doi.org/10.1088/1538-3873/aae8ac)
- Miller, A. A., Yao, Y., Bulla, M., et al. 2020, *ApJ*, 902, 47, doi: [10.3847/1538-4357/abb13b](https://doi.org/10.3847/1538-4357/abb13b)
- Nicolas, N., Rigault, M., Copin, Y., et al. 2021, *A&A*, 649, A74, doi: [10.1051/0004-6361/202038447](https://doi.org/10.1051/0004-6361/202038447)
- Nomoto, K. 1980, *SSRv*, 27, 563, doi: [10.1007/BF00168350](https://doi.org/10.1007/BF00168350)
- Nomoto, K., Iwamoto, K., Nakasato, N., et al. 1997, *NuPhA*, 621, 467, doi: [10.1016/S0375-9474\(97\)00291-1](https://doi.org/10.1016/S0375-9474(97)00291-1)
- Olling, R. P., Mushotzky, R., Shaya, E. J., et al. 2015, *Nature*, 521, 332, doi: [10.1038/nature14455](https://doi.org/10.1038/nature14455)
- Pan, Y. C., Jheng, Y. S., Jones, D. O., et al. 2022, arXiv e-prints, arXiv:2211.06895, doi: [10.48550/arXiv.2211.06895](https://doi.org/10.48550/arXiv.2211.06895)



- Perlmutter, S., Aldering, G., Goldhaber, G., et al. 1999, ApJ, 517, 565, doi: [10.1086/307221](https://doi.org/10.1086/307221)
- Piersanti, L., Gagliardi, S., Iben, Icko, J., & Tornambé, A. 2003, ApJ, 598, 1229, doi: [10.1086/378952](https://doi.org/10.1086/378952)
- Piro, A. L. 2012, ApJ, 759, 83, doi: [10.1088/0004-637X/759/2/83](https://doi.org/10.1088/0004-637X/759/2/83)
- Piro, A. L., & Morozova, V. S. 2016, ApJ, 826, 96, doi: [10.3847/0004-637X/826/1/96](https://doi.org/10.3847/0004-637X/826/1/96)
- Piro, A. L., & Nakar, E. 2013, ApJ, 769, 67, doi: [10.1088/0004-637X/769/1/67](https://doi.org/10.1088/0004-637X/769/1/67)
- Planck Collaboration, Aghanim, N., Akrami, Y., et al. 2018, ArXiv e-prints. <https://arxiv.org/abs/1807.06209>
- Polin, A., Nugent, P., & Kasen, D. 2019, ApJ, 873, 84, doi: [10.3847/1538-4357/aafb6a](https://doi.org/10.3847/1538-4357/aafb6a)
- Riess, A. G., Filippenko, A. V., Challis, P., et al. 1998, AJ, 116, 1009, doi: [10.1086/300499](https://doi.org/10.1086/300499)
- Riess, A. G., Filippenko, A. V., Li, W., et al. 1999, AJ, 118, 2675, doi: [10.1086/301143](https://doi.org/10.1086/301143)
- Riess, A. G., Macri, L. M., Hoffmann, S. L., et al. 2016, ApJ, 826, 56, doi: [10.3847/0004-637X/826/1/56](https://doi.org/10.3847/0004-637X/826/1/56)
- Riess, A. G., Yuan, W., Macri, L. M., et al. 2022, ApJL, 934, L7, doi: [10.3847/2041-8213/ac5c5b](https://doi.org/10.3847/2041-8213/ac5c5b)
- Rigault, M., Brinnel, V., Aldering, G., et al. 2020, A&A, 644, A176, doi: [10.1051/0004-6361/201730404](https://doi.org/10.1051/0004-6361/201730404)
- Rose, B. M., Garnavich, P. M., & Berg, M. A. 2019, arXiv e-prints. <https://arxiv.org/abs/1902.01433>
- Rubin, D., Aldering, G., Betoule, M., et al. 2023, arXiv e-prints, arXiv:2311.12098, doi: [10.48550/arXiv.2311.12098](https://doi.org/10.48550/arXiv.2311.12098)
- Schlafly, E. F., & Finkbeiner, D. P. 2011, ApJ, 737, 103, doi: [10.1088/0004-637X/737/2/103](https://doi.org/10.1088/0004-637X/737/2/103)
- Scolnic, D., Brout, D., Carr, A., et al. 2022, ApJ, 938, 113, doi: [10.3847/1538-4357/ac8b7a](https://doi.org/10.3847/1538-4357/ac8b7a)
- Scolnic, D. M., Jones, D. O., Rest, A., et al. 2018, ApJ, 859, 101, doi: [10.3847/1538-4357/aab9bb](https://doi.org/10.3847/1538-4357/aab9bb)
- Shappee, B. J., Piro, A. L., Stanek, K. Z., et al. 2018, ApJ, 855, 6, doi: [10.3847/1538-4357/aaa1e9](https://doi.org/10.3847/1538-4357/aaa1e9)
- Shappee, B. J., Piro, A. L., Holoiën, T. W. S., et al. 2016, ApJ, 826, 144, doi: [10.3847/0004-637X/826/2/144](https://doi.org/10.3847/0004-637X/826/2/144)
- Shappee, B. J., Holoiën, T. W. S., Drout, M. R., et al. 2019, ApJ, 870, 13, doi: [10.3847/1538-4357/aaec79](https://doi.org/10.3847/1538-4357/aaec79)
- Siverd, R. J., Goobar, A., Stassun, K. G., & Pepper, J. 2015, ApJ, 799, 105, doi: [10.1088/0004-637X/799/1/105](https://doi.org/10.1088/0004-637X/799/1/105)
- Srivastav, S., Smartt, S. J., Huber, M. E., et al. 2023, ApJL, 943, L20, doi: [10.3847/2041-8213/acb2ce](https://doi.org/10.3847/2041-8213/acb2ce)
- Stritzinger, M. D., Shappee, B. J., Piro, A. L., et al. 2018, ApJL, 864, L35, doi: [10.3847/2041-8213/aadd46](https://doi.org/10.3847/2041-8213/aadd46)
- Sullivan, M., Conley, A., Howell, D. A., et al. 2010, MNRAS, 406, 782, doi: [10.1111/j.1365-2966.2010.16731.x](https://doi.org/10.1111/j.1365-2966.2010.16731.x)
- Sullivan, M., Guy, J., Conley, A., et al. 2011, ApJ, 737, 102, doi: [10.1088/0004-637X/737/2/102](https://doi.org/10.1088/0004-637X/737/2/102)
- Taylor, E. N., Hopkins, A. M., Baldry, I. K., et al. 2011, MNRAS, 418, 1587, doi: [10.1111/j.1365-2966.2011.19536.x](https://doi.org/10.1111/j.1365-2966.2011.19536.x)
- Taylor, G., Jones, D. O., Popovic, B., et al. 2023, MNRAS, 520, 5209, doi: [10.1093/mnras/stad320](https://doi.org/10.1093/mnras/stad320)
- Thorp, S., & Mandel, K. S. 2022, MNRAS, 517, 2360, doi: [10.1093/mnras/stac2714](https://doi.org/10.1093/mnras/stac2714)
- Tonry, J. L., Denneau, L., Heinze, A. N., et al. 2018, PASP, 130, 064505, doi: [10.1088/1538-3873/aabadf](https://doi.org/10.1088/1538-3873/aabadf)
- Tripp, R. 1998, A&A, 331, 815
- Uddin, S. A., Burns, C. R., Phillips, M. M., et al. 2023, arXiv e-prints, arXiv:2308.01875, doi: [10.48550/arXiv.2308.01875](https://doi.org/10.48550/arXiv.2308.01875)
- van Kerkwijk, M. H., Chang, P., & Justham, S. 2010, ApJL, 722, L157, doi: [10.1088/2041-8205/722/2/L157](https://doi.org/10.1088/2041-8205/722/2/L157)
- Virtanen, P., Gommers, R., Oliphant, T. E., et al. 2020, Nature Methods, 17, 261, doi: [10.1038/s41592-019-0686-2](https://doi.org/10.1038/s41592-019-0686-2)
- Wang, Q., Rest, A., Dimitriadis, G., et al. 2023, arXiv e-prints, arXiv:2305.03779, doi: [10.48550/arXiv.2305.03779](https://doi.org/10.48550/arXiv.2305.03779)
- Webbink, R. F. 1984, ApJ, 277, 355, doi: [10.1086/161701](https://doi.org/10.1086/161701)
- Whelan, J., & Iben, Icko, J. 1973, ApJ, 186, 1007, doi: [10.1086/152565](https://doi.org/10.1086/152565)
- Wiseman, P., Sullivan, M., Smith, M., & Popovic, B. 2023, MNRAS, 520, 6214, doi: [10.1093/mnras/stad488](https://doi.org/10.1093/mnras/stad488)
- Wiseman, P., Sullivan, M., Smith, M., et al. 2021, MNRAS, 506, 3330, doi: [10.1093/mnras/stab1943](https://doi.org/10.1093/mnras/stab1943)
- Woosley, S. E., & Weaver, T. A. 1994, ApJ, 423, 371, doi: [10.1086/173813](https://doi.org/10.1086/173813)
- Yao, Y., Miller, A. A., Kulkarni, S. R., et al. 2019, ApJ, 886, 152, doi: [10.3847/1538-4357/ab4cf5](https://doi.org/10.3847/1538-4357/ab4cf5)
- York, D. G., Adelman, J., Anderson, John E., J., et al. 2000, AJ, 120, 1579, doi: [10.1086/301513](https://doi.org/10.1086/301513)